DTIC FILE COPY

CRREL
REPORT 89-11

④

89 7 25 049

AD–A210 484

Thermal and size evolution of
sea spray droplets

DTIC
ELECTE
JUL 2 5 1989
S E D

CRREL Report 89-11

June 1989

Thermal and size evolution of sea spray droplets

Edgar L Andreas

REPORT DOCUMENTATION PAGE

Form Approved
OMB NO. 0704-0188
Exp. Date: Jun 30, 1986

1a. REPORT SECURITY CLASSIFICATION Unclassified	1B. RESTRICTIVE MARKINGS
2a. SECURITY CLASSIFICATION AUTHORITY	3. DISTRIBUTION/AVAILABILITY OF REPORT Approved for public release; distribution is unlimited.
2b. DECLASSIFICATION/DOWNGRADING SCHEDULE	

4. PERFORMING ORGANIZATION REPORT NUMBER(S) CRREL Report 89-11	5. MONITORING ORGANIZATION REPORT NUMBER(S)

6a. NAME OF PERFORMING ORGANIZATION U.S. Army Cold Regions Research and Engineering Laboratory	6b. OFFICE SYMBOL *(if applicable)* CECRL	7a. NAME OF MONITORING ORGANIZATION Office of Naval Research
6c. ADDRESS *(City, State, and ZIP Code)* 72 Lyme Road Hanover, N.H. 03755-1290		7b. ADDRESS *(City, State, and ZIP Code)* 800 North Quincy Street Arlington, Virginia 22217-5000

8a. NAME OF FUNDING/SPONSORING ORGANIZATION	8b. OFFICE SYMBOL *(if applicable)*	9. PROCUREMENT INSTRUMENT IDENTIFICATION NUMBER N0001986MP67847 N0001488WM22012 N0001489WM22006

8c. ADDRESS *(City, State, and ZIP Code)*	10. SOURCE OF FUNDING NUMBERS			
	PROGRAM ELEMENT NO.	PROJECT NO.	TASK NO.	WORK UNIT ACCESSION NO.

11. TITLE *(Include Security Classification)*

Thermal and Size Evolution of Sea Spray Droplets

12. PERSONAL AUTHOR(S)
Edgar L Andreas

13a. TYPE OF REPORT	13b. TIME COVERED FROM _____ TO _____	14. DATE OF REPORT *(Year, Month, Day)* June 1989	15. PAGE COUNT 48

16. SUPPLEMENTARY NOTATION

17.	COSATI CODES		18. SUBJECT TERMS *(Continue on reverse if necessary and identify by block number)*
FIELD	GROUP	SUB-GROUP	Air–sea interaction Microphysics Sea spray
			Bubbles Moisture transfer Water droplets
			Heat transfer Polar lows Whitecaps

19. ABSTRACT *(Continue on reverse if necessary and identify by block number)*

Sea spray droplets initially have the same temperature as the ocean surface from which they formed. In high latitudes, under a relatively cold wind, they therefore cool and evaporate, in effect enhancing the air–sea exchange of heat and moisture. With a future goal of investigating this enhanced exchange in mind, this report develops model equations with which to track the thermal and size (moisture content) evolution of a spray droplet from the time it is created until it comes to equilibrium with its environment. On testing the model against some of the scanty data available on the evolution of saline droplets, good agreement is found. The thermal evolution of the droplets obeys $T(t)-T_{eq} \propto \exp(-t/\tau_T)$ very well. Here, T is the instantaneous droplet temperature, T_{eq} is the equilibrium temperature of the droplet and t is time. The time constant τ_T is the time required for the droplet to come to within e^{-1} of T_{eq}. Similarly, for the moisture (size or radius) evolution, a time scale τ_r is defined as the time required for the droplet radius to come to within e^{-1} of its equilibrium radius. τ_r is always about three orders of magnitude larger than τ_T; the thermal exchange is thus virtually complete before the moisture transfer starts. Consequently, the ambient humidity has little effect on the thermal exchange, and, analogously, the initial droplet temperature has neglible effect on the moisture exchange.

20. DISTRIBUTION/AVAILABILITY OF ABSTRACT ☒ UNCLASSIFIED/UNLIMITED ☐ SAME AS RPT. ☐ DTIC USERS	21. ABSTRACT SECURITY CLASSIFICATION Unclassified	
22a. NAME OF RESPONSIBLE INDIVIDUAL Edgar L Andreas	22b. TELEPHONE *(Include Area Code)* 603-646-4100	22c. OFFICE SYMBOL CECRL-RS

DD FORM 1473, 84 MAR

83 APR edition may be used until exhausted.
All other editions are obsolete.

PREFACE

CONTENTS

Page

ILLUSTRATIONS

Figure

NOMENCLATURE

a acceleration of a falling sea spray droplet

a_w $e_{sat,s}/e_{sat}$, the water activity of an aqueous solution

B function of r_{80} in the spray generation function of Monahan et al. (1986)

c molar concentration of an aqueous solution

C_D drag coefficient of a spray droplet

c_{pa} 1.006×10^3 J kg^{-1} $^\circ$C^{-1}, the specific heat of air at constant pressure

c_{ps} 4.0×10^3 J kg^{-1} $^\circ$C^{-1}, the specific heat of a spray droplet (i.e., of sea water) at constant pressure

dF/dr spray generation function; number of droplets produced at the sea surface per unit surface area per unit time per unit increment in initial droplet radius

dF/dr_{80} spray generation function when all droplets are brought to a relative humidity of 80%

dF_0/dr_{80} contribution to dF/dr_{80} from bursting bubbles; droplet sizes referenced to a standard humidity of 80%

dF_1/dr_{80} contribution to dF/dr_{80} from spume droplets; droplet sizes referenced to a standard humidity of 80%

D_h 1.4×10^{-7} m^2/s, diffusivity of heat in sea water at 0°C

D_s 6.8×10^{-10} m^2/s, diffusivity of NaCl in sea water at 0°C

D_w bulk molecular diffusivity of water vapor in air

D_w' water vapor diffusivity in air modified for noncontinuum effects

e_{sat} pressure of water vapor in saturation with a plane surface of pure water

$e_{sat,s}$ pressure of water vapor in saturation with the plane surface of an aqueous solution

f RH/100, fractional relative humidity

f_x rate of change of the variable x with time

f_0 $1 - 0.000537\,S$, fractional relative humidity at the sea surface

g 9.82 m/s, acceleration due to gravity

$g(f)$ function in Fitzgerald's (1975) model of droplet size

k_a thermal conductivity of air

k_a' thermal conductivity of air modified for noncontinuum effects

L_v latent heat of vaporization of water

m molality of a solution

M_a 28.9644×10^{-3} kg/mol, molecular weight of air

m_{d0} initial mass of a sea spray droplet

M_s 58.443×10^{-3} kg/mol, molecular weight of sodium chloride

m_s mass of salt contained by a spray droplet

M_w 18.0160×10^{-3} kg/mol, molecular weight of water

m_w mass of water contained by a spray droplet

m_{w0} initial mass of water contained by a spray droplet

P	atmospheric pressure
P_0	1013.25 hPa, standard atmospheric pressure
R	8.31441 J mol^{-1} K^{-1}, universal gas constant
r	radius of a sea spray droplet
r_d	radius of the (dry) salt particle left when a spray droplet evaporates
r_{eq}	radius of a droplet in equilibrium with its environment
r_0	initial radius of a sea spray droplet
r_{80}	radius of a droplet in equilibrium with an environment at 80% relative humidity
Re	Reynolds number of a droplet
RH	100 f, relative humidity
S	surface salinity of the ocean
S_d	instantaneous salinity of a spray droplet
$S_v{}^*$	function of temperature used in finding the apparent molal volume of an aqueous solution
T	instantaneous droplet temperature or any general temperature
t	time
T_a	air temperature
T_{eq}	temperature of a droplet in thermal equilibrium with its environment
T_w	surface temperature of the ocean
T_0	273.15 K (= 0°C), the ice point
U	wind speed at a reference height of 10 m
u	instantaneous speed at which a droplet is falling
u_f	terminal fall speed of a droplet
v_a	apparent molal volume of an aqueous solution
v_{a0}	apparent molal volume of a solution at infinite dilution
x	either r or T
x_n	discrete value of x at time step n
y	function that gives the effects of curvature and dissolved salt on the vapor pressure at the surface of a spray droplet
α	function of f in Fitzgerald's (1975) model of droplet size
α_c	0.036, a dimensionless constant used in computing the modified water vapor diffusivity
α_T	0.7, a dimensionless constant used in computing the modified thermal conductivity
β	function of f in Fitzgerald's (1975) model of droplet size
δ	$(T/T_a) - 1$, see eq 2
Δ_T	2.17 × 10^{-7} m, a length scale used in computing the modified thermal conductivity
Δ_w	8 × 10^{-8} m, a length scale used in computing the modified water vapor diffusivity
Δt	time step
λ	mean free path of air molecules
ν	2, the number of ions into which a sodium chloride molecule dissociates
ν_a	kinematic viscosity of air
ρ_a	density of air
ρ_s	solution density of a spray droplet
ρ_{s0}	initial solution density of a spray droplet
ρ_v	ambient water vapor density

ρ_{vr} water vapor density at the surface of a spray droplet of radius r

ρ_w density of pure water

σ_s surface tension of a plane, aqueous solution

σ_w surface tension of a plane, pure water solution

τ_f time required for a spray droplet with terminal fall speed u_t to fall 1 m in still air

τ_h time required for the interior of a spray droplet to be everywhere within 4% of an impulsively applied surface temperature

τ_r time required for a spray droplet to come to within e^{-1} of its equilibrium radius

τ_T time required for a spray droplet to come to within e^{-1} of its equilibrium temperature

τ_{Tc} τ_T value estimated from eq 74

τ_s upper bound on the time required for excess salt at a droplet surface to diffuse throughout the interior of the droplet

ϕ_n time derivative of either r or T at time step n

$\hat{\phi}$ $(\phi_n + \phi_{n+1})/2$

Φ_s practical osmotic coefficient of sodium chloride dissolved in water

Thermal And Size Evolution Of Sea Spray Droplets

EDGAR L ANDREAS

INTRODUCTION

As the wind speed at a height of 10 m reaches 3–4 m/s, the ocean surface becomes disrupted—whitecapping begins (Monahan 1971, Wu 1979, Monahan and Ó Muircheartaigh 1981, Monahan et al. 1983). These whitecaps form when clouds of air bubbles that were trapped by breaking waves rise to the surface and burst. The bursting bubbles, in turn, throw sea spray droplets into the air. When the wind speed reaches 9 m/s, a second mechanism for generating sea spray comes into play. Now the wind is strong enough to tear off the wave crests and to propel spray directly into the air (Monahan et al. 1986).

The effects attributable to this spray are manifold. For example, spray droplets can carry electrostatic charges away from the sea surface; the resulting atmospheric electrification can manifest elsewhere as a thunderstorm (Blanchard 1963, Roll 1965). Spray droplets can transport organic matter, such as bacteria, from the sea to the air (Blanchard 1983). Sea spray droplets are saline; when a droplet evaporates, it leaves behind a microscopic sea-salt particle that the wind can easily carry long distances. These sea-salt particles are common cloud condensation nuclei (Woodcock 1952, Mason 1957, Cipriano et al. 1987) and are also implicated as condensation nuclei for marine fogs (Woodcock 1978). If the sea-salt aerosol encounters a more humid environment, the particles can become rewetted to form marine haze, which affects the extinction of electromagnetic waves propagating in the marine boundary layer (Schacher et al. 1981).

As the wind speed increases, the number of spray droplets produced increases by several orders of magnitude. As a result, in high winds, sea spray droplets—which start at the temperature of the ocean surface—effectively increase the oceanic surface area. Spray thus has the potential for enhancing the transfer of all constituents that are typically exchanged at the air–sea interface. The most important of these constituents are sensible heat, latent heat (moisture) and gases. Several authors have already looked at the impact of sea spray on heat and moisture transfer across the air–sea interface (Bortkovskii 1973, 1987, Borisenkov 1974, Wu 1974, Ling and Kao 1976, Ling et al. 1978, Wang and Street 1978, Street et al. 1978, Mestayer and Lefauconnier 1988) but have reached no consensus as to if or when the spray transfer is important or on how to parameterize its magnitude. In general, most agree that in high winds (> 15 m/s), the sea spray must enhance the interfacial transfers of heat and moisture, but the magnitude of the effect is unknown.

I, too, am interested in what impact sea spray has on air–sea heat and moisture transfer, especially over the high latitude ocean. Here, enormous sensible and latent heat fluxes occur when air flowing off the cold pack ice encounters the relatively warm ocean. These fluxes provide energy for the generation and maintenance of polar lows (Rasmus-

sen 1985, Shapiro et al. 1987), small synoptic or subsynoptic-scale cyclones that form in the ice edge region and intensify as they move over the relatively warm waters of the open ocean (Kellogg and Twitchell 1986, Rasmussen and Lystad 1987). The high winds associated with polar lows, of course, produce sea spray; this spray may, in turn, feed heat and moisture back into the system and, thus, further intensify it. My long-range objective is to quantify the magnitude of this feedback.

The thermodynamics of sea spray droplets at high latitudes is conceptually simple (Fig. 1). When a cold wind blowing off the pack ice encounters the relatively warm ocean, it fosters intense, upward turbulent fluxes of sensible and latent heat at the air–sea interface. By disrupting the sea surface, the wind also produces spray droplets. Since these droplets must initially have the same temperature as the ocean surface, they transfer additional sensible heat to the air as they cool. The droplets also begin evaporating because the cold air generally has low absolute humidity. This evaporation must extract latent heat from the air but also provides water vapor to the atmospheric boundary layer, thereby increasing its humidity and providing vapor that immediately condenses to fog or can easily rise to higher altitudes to form clouds.

Although conceptually simple, sea spray thermodynamics is parametrically complex. The number and size of the spray droplets produced depend on the wind speed and, to some extent, on the air and sea temperatures. The evolution of the temperature and size (radius or moisture content) of a spray droplet depends on its size, on the air and sea temperatures, on the ambient humidity, on the surface salinity of the ocean, and on the wind speed and the associated turbulent wind field in the atmospheric surface layer. In addition, in the ice edge region, the environment in which the spray droplets evolve is not horizontally homogeneous or in steady state. As the air flows off the ice and over the open ocean, oceanic heat and moisture continually warm and moisten it.

To simplify the analysis for this initial report, I will focus on the thermodynamics of individual sea spray droplets in a steady-state environment. Pruppacher and Klett (1978) developed equations for the rates of change of the temperature and radius of cloud droplets. I use, basically, their equations to investigate the thermal and size evolution of saline sea spray droplets. Earlier, Andreas et al. (1981) had also used Pruppacher and Klett's equations to model the evolution of condensate droplets. Ultimately, I parameterize the evolution of sea spray droplets in terms of e-folding times—the times necessary for a
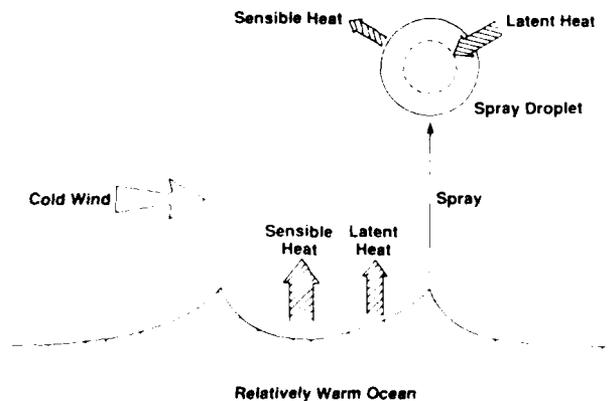
Figure 1. Conceptual model of heat and moisture transfer associated with sea spray.

2

droplet to come to within e^{-1} of its equilibrium temperature and equilibrium radius for the given ambient conditions. On comparing these times with typical Stokes fall rates, we get some idea of the size range of spray droplets that can most effectively participate in the heat transfer. The spray generation function proposed by Monahan et al. (1986) provides the necessary information on the size of spray droplets and on the rate at which they are produced.

SIZE EVOLUTION EQUATION

In their Chapter 13, Pruppacher and Klett (1978) developed a rate equation for the change in radius of an aqueous solution droplet. Their development culminates with eq (13-26), which I repeat here

$$r\frac{dr}{dt} = \frac{D_w' M_w e_{sat}(T_a)}{\rho_s R T_a} \left\{ f - \frac{1}{1+\delta} \exp\left[\frac{L_v M_w}{RT_a}\left(\frac{\delta}{1+\delta}\right) + \frac{2M_w \sigma_s}{RT_a(1+\delta)\rho_w r} - \frac{v\Phi_s m_s(M_w/M_s)}{(4\pi r^3 \rho_s/3)-m_s} \right] \right\}$$

(1)

$$\qquad\qquad\quad \text{I} \qquad\qquad\qquad\qquad \text{II} \qquad\qquad \text{III} \qquad\qquad \text{IV}$$

where r = instantaneous radius of the spray droplet at time t
ρ_s = density of the droplet
ρ_w = density of pure water
m_s = mass of NaCl in the droplet
D_w' = modified molecular diffusivity of water vapor in air
R = universal gas constant
L_v = latent heat of vaporization of water
M_w = molecular weight of water
M_s = molecular weight of NaCl
T_a = ambient air temperature
f = fractional relative humidity (e.g., if $RH = 80\%$, $f = 0.80$)
$e_{sat}(T_a)$ = saturation vapor pressure over a pure, flat water surface with temperature T_a
σ_s = surface tension of a flat surface with the same salinity and temperature as the spray droplet
Φ_s = practical osmotic coefficient of the droplet
v = total number of ions into which a salt molecule in the droplet dissociates.
And

$$\delta = \frac{T}{T_a} - 1 = \frac{L_v \rho_s}{T_a k_a'}\, r\frac{dr}{dt}$$

(2)

where T is the instantaneous droplet temperature (assumed uniform), and k_a' is the modified thermal conductivity of air. Although sea water contains measurable amounts of many dissolved salts, sodium chloride, NaCl, is by far the main component (Neumann and Pierson 1966). Henceforth, I assume that sea spray droplets contain only NaCl as a solute; v is thus 2.

3

The *Nomenclature* lists all of these symbols and gives the values of the ones that are constants. As we go on, the meanings of some of the less familiar ones should become clearer.

Before simplifying eq 1, let me interpret the terms so we can see what affects the moisture content of a spray droplet. In eq 1, term I, the ambient humidity, is the main term driving the diffusion of water vapor toward or away from the droplet. This, compared with the humidity at the exact surface of the droplet, dictates in which direction the vapor diffuses. Terms II, III and IV predict the humidity at the droplet surface and show that three distinct phenomena affect it. Term II results because the droplet is not at the ambient air temperature; therefore, its surface vapor pressure is computed at T rather that at T_a. Once a droplet reaches thermal equilibrium, if the droplet is evaporating, it must be cooler than the air because the vapor is carrying away latent heat. Conversely, if vapor is condensing on the droplet, it must be warmer than the ambient air. Term III reflects the effects of surface tension and droplet curvature. An increase in this term increases the vapor pressure at the droplet surface and thereby enhances evaporation but retards condensation. Notice the r^{-1} dependence in term III—the term becomes increasingly important as the droplet radius decreases. Term IV reflects the fact that salts dissolved in the droplet depress its surface vapor pressure.

Since $|\delta|$ is rarely larger than 0.1, in eq 1 we can approximate

$$\frac{1}{1+\delta} \approx 1-\delta \tag{3}$$

$$\exp\left[\frac{L_v M_w}{RT_a}\left(\frac{\delta}{1+\delta}\right)\right] \approx \exp\left[\frac{L_v M_w \delta}{R T_a}\right]$$
$$\approx 1 + \frac{L_v M_w \delta}{R T_a} \tag{4}$$

and

$$\frac{2 M_w \sigma_s}{R T_a (1+\delta) \rho_w r} \approx \frac{2 M_w \sigma_s}{R T_a \rho_w r}. \tag{5}$$

Thus, eq 1 becomes

$$r\frac{dr}{dt} = \frac{D_w' M_w e_{sat}(T_a)}{\rho_s R T_a}\left[f - (1-\delta)\left(1 + \frac{L_v M_w \delta}{R T_a}\right)\exp(y)\right] \tag{6}$$

where

$$y = \frac{2 M_w \sigma_s}{R T_a \rho_w r} - \frac{v \, \Phi_s \, m_s \, (M_w/M_s)}{(4\pi r^3 \rho_s /3) - m_s}. \tag{7}$$

Since surface tension and solute effects are small for many spray droplets in the size range we are considering (Pruppacher and Klett 1978, p. 420), y is small. Therefore, we also approximate

$$\exp(y) \approx 1 + y. \tag{8}$$

4

Substituting this in eq 6, multiplying out the products and discarding terms containing second and higher order terms (i.e., δ^2, δy and $\delta^2 y$), we obtain

$$r\frac{dr}{dt} = \frac{D_w{'}\,M_w\,e_{sat}\,(T_a)}{\rho_s\,R\,T_a}\left[(f-1)+\delta\left(1-\frac{L_v\,M_w}{R\,T_a}\right)-y\right]. \tag{9}$$

Because δ contains $r(dr/dt)$ (see eq 2), we can solve eq 9 for the rate of change of the spray droplet radius, dr/dt. The result is

$$\frac{dr}{dt} = \frac{\left[(f-1)-y\right]r^{-1}}{\dfrac{\rho_s\,R\,T_a}{D_w{'}\,M_w\,e_{sat}\,(T_a)}+\dfrac{L_v\,\rho_s}{T_a\,k_a{'}}\left(\dfrac{L_v\,M_w}{R\,T_a}-1\right)}. \tag{10}$$

Notice, implicit in this result is the condition for a droplet to be in moisture equilibrium with its environment. This occurs when

$$f-1 = y. \tag{11}$$

That is, the relative humidity is dominant in determining the equilibrium radius. But the mass of the salt contained in the droplet m_s, the air temperature T_a, and the equilibrium droplet temperature, which affects ρ_w, ρ_s and σ_s, are also important.

In the *Numerical Methods* section, I will present a numerical technique for solving this equation for the droplet radius as a function of time. In the remainder of this section, I will discuss the equations I use to compute the physical and chemical variables necessary to employ eq 10.

The ambient environmental parameters that I specify before solving eq 10 are the air temperature T_a, the relative humidity RH ($= 100\,f$), the sea surface temperature T_w, the sea surface salinity S and the atmospheric pressure P. I also specify the initial radius of the spray droplet r_0—the radius at the instant it is created at the ocean surface. Lastly, I assume that the initial droplet temperature is T_w.

According to Pruppacher and Klett (1978, p. 87)

$$\rho_s = \rho_w\frac{1+\dfrac{m_s}{m_w}}{1+v_a\dfrac{\rho_w}{M_s}\dfrac{m_s}{m_w}} \tag{12}$$

where m_w is the mass of pure water in the droplet and v_a is the apparent molal volume of the solution droplet. I compute the density of pure water in kilograms per cubic meter at droplet temperature T from (Pruppacher and Klett 1978, p. 86)

$$\rho_w = \frac{999.8396 + 18.224944\,T - 7.922210\times 10^{-3}\,T^2}{1+1.8159725\times 10^{-2}\,T}\quad\text{for }0\le T\le 40^\circ\text{C} \tag{13a}$$

$$\rho_w = 999.84 + 8.60\times 10^{-2}\,T - 1.08\times 10^{-2}\,T^2\text{ for}-50\le T\le 0^\circ\text{C}. \tag{13b}$$

5

The apparent molal volume v_a in eq 12 reflects the effects of the dissolved salt on the density of the aqueous solution droplet and thereby parameterizes deviations from an ideal solution. Millero (1972) discussed the Masson relationship

$$v_a = v_{a0} + S_v{}^* c^{1/2} \tag{14}$$

which gives v_a as a function of the apparent molal volume at infinite dilution v_{a0}, an experimental slope $S_v{}^*$, and the molar concentration of the salt in moles per liter

$$c = 10^{-3} \frac{m_s/M_s}{4\pi r^3/3}. \tag{15}$$

Here the denominator is the droplet volume; the factor 10^{-3} converts moles per cubic meter to moles per liter required in eq 14. v_{a0} and $S_v{}^*$ depend on the solute and on the droplet temperature. To determine what they are for NaCl, I plotted Millero's data and fitted them with polynomials (Fig. 2 and 3). In tabulating his v_{a0} data, Millero indicated the values that he felt were most reliable. I fitted the polynomial to these data only; the resulting prediction for v_{a0} in cubic meters per mole for $0 \le T \le 55°C$ is

$$10^6 v_{a0} = 12.97 + 0.2340\,T - 4.210 \times 10^{-3}\,T^2 + 2.857 \times 10^{-5}\,T^3. \tag{16}$$

For $S_v{}^*$ in $m^3\,L^{1/2}\,mol^{-3/2}$, my polynomial fit for $0 \le T \le 100°C$ is

$$10^6 S_v{}^* = 2.982 - 4.970 \times 10^{-2}\,T + 6.032 \times 10^{-4}\,T^2. \tag{17}$$
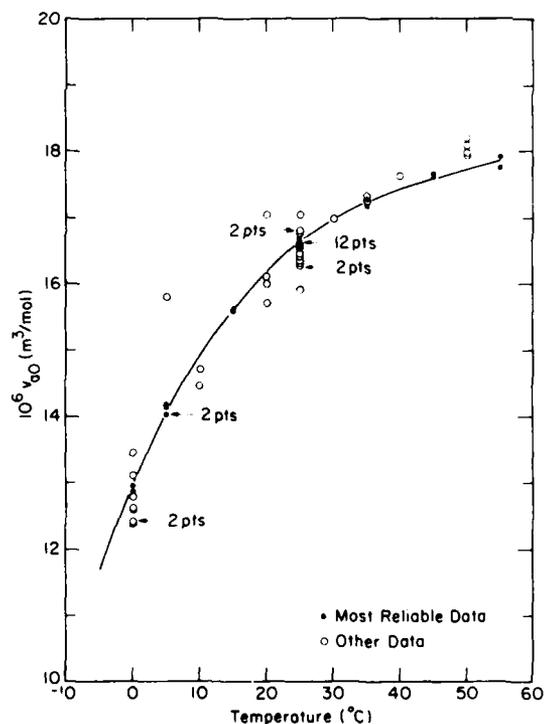
Figure 2. Apparent molal volume at infinite dilution for NaCl dissolved in pure water. The data are from Millero (1972); the curve is eq 16.

6
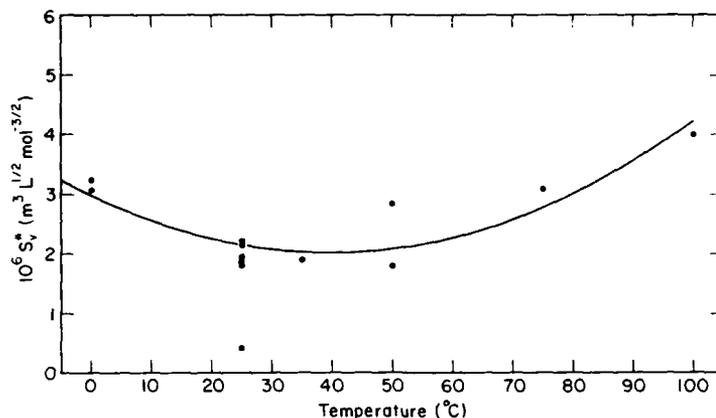
Figure 3. Slope in the Masson equation (eq 14) for NaCl dissolved in pure water. The data are from Millero (1972); the curve is eq 17.

Notice that in Figures 2 and 3 the available data are all above 0°C; my polynomials, eq 16 and 17, thus have the same lower limit. At high latitudes, however, supercooled sea spray droplets commonly exist. My only alternative for modeling these droplets is to hope that eq 16 and 17 are adequate on extrapolation below 0°C.

The instantaneous salinity of the droplet S_d is given by

$$S_d = \frac{m_s}{m_w + m_s} .$$

(18)

Consequently,

$$S = \frac{m_s}{m_{w0} + m_s}$$

(19)

where m_{w0} is the initial mass of pure water in the droplet. Because

$$\frac{m_s}{m_{w0}} = \frac{S}{1-S}$$

(20)

we can compute the initial droplet density from eq 12 if we approximate

$$m_s \approx \frac{4}{3} \pi \rho_w r_0^3 \frac{m_s}{m_{w0}}$$

(21)

for use in eq 15. Calculating the initial droplet density ρ_{s0} and chosing an initial radius r_0, we can find the initial droplet mass

$$m_{d0} = \frac{4}{3} \pi \rho_{s0} r_0^3 .$$

(22)

Since

$$m_{d0} = m_{w0} + m_s$$

(23)

7

we see from eq 20 that the mass of salt in the droplet is

$$m_s = S\, m_{d0} \tag{24}$$

which is assumed to be constant for the lifetime of the droplet.

The practical osmotic coefficient Φ_s in eq 7 quantifies how dissolved salts affect the saturation vapor pressure $e_{sat,s}$ at a plane solution surface. Φ_s is related to the water activity $a_w = e_{sat,s}/e_{sat}$ by (Pruppacher and Klett 1978, p. 82)

$$-\ln a_w = v\, m\, M_w\, \Phi_s . \tag{25}$$

Here m is a concentration unit, the molality—the number of moles of salt dissolved in 1 kg of water

$$m = \frac{m_s}{M_s\, m_w} . \tag{26}$$

Low (1969a, 1969b) tabulated a_w as a function of m for sodium chloride dissolved in water at 25°C. I converted his a_w values to Φ_s according to eq 25 and plotted these in Figure 4. The least-squares polynomial I have fitted to these data is

$$\Phi_s = 0.9270 - 2.164 \times 10^{-2}\, m + 3.486 \times 10^{-2}\, m^2$$

$$- 5.956 \times 10^{-3}\, m^3 + 3.911 \times 10^{-4}\, m^4 \tag{27}$$

for $0 \le m \le 6$.
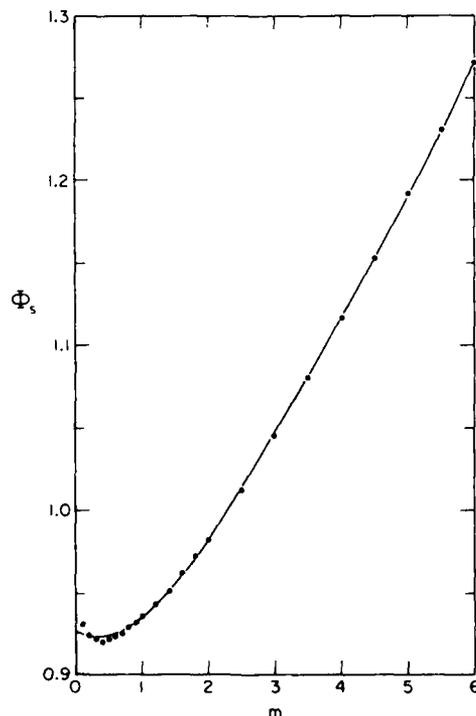
Figure 4. Practical osmotic coefficient of NaCl dissolved in water as a function of the molality. Data are from Low (1969a, 1969b); the curve is eq 27.

8

In the transfer of heat and moisture in the immediate vicinity of microscopic spray droplets, the air need not act as a continuum; eq 10, therefore, contains modified values of the molecular diffusivity of water vapor in air D_w' and the thermal conductivity of air k_a'. From Pruppacher and Klett (1978, p. 415)

$$D_w' = \left[\frac{D_w(T)}{\frac{r}{r+\Delta_w}+\frac{D_w(T)}{r\,\alpha_c}\left(\frac{2\,\pi\,M_w}{R\,T}\right)^{1/2}}\right].$$

(28)

Here $\alpha_c = 0.036$ and $\Delta_w = 1.3\lambda = 8 \times 10^{-8}$ m are empirical constants, where λ is the mean free path of air molecules. I compute the bulk diffusivity D_w at the droplet temperature T and the atmospheric pressure P from (Pruppacher and Klett 1978, p. 413)

$$D_w = 2.11 \times 10^{-5}\left(\frac{T}{T_0}\right)^{1.94}\left(\frac{P_0}{P}\right)$$

(29)

which gives D_w in square meters per second for $T_0 = 273.15$ K and $P_0 = 1013.25$ hPa.

Pruppacher and Klett (1978, p. 418) gave an analogous expression for the modified thermal conductivity

$$k_a' = \left[\frac{k_a(T)}{\frac{r}{r+\Delta_T}+\frac{k_a(T)}{r\,\alpha_T\,\rho_a c_{pa}}\left(\frac{2\,\pi\,M_a}{R\,T}\right)^{1/2}}\right].$$

(30)

Again $\alpha_T = 0.7$ and $\Delta_T = 2.16 \times 10^{-7}$ m are empirical constants. Also $c_{pa} = 1.006 \times 10^3$ J kg^{-1} °C^{-1} is the specific heat of air at constant pressure, and

$$\rho_a = 1.2923\left(\frac{T_0}{T}\right)\left(\frac{P}{P_0}\right)$$

(31)

is the density of air in kilograms per cubic meter at the droplet temperature.

I compute the thermal conductivity of bulk air k_a at the droplet temperature T using a polynomial I fitted to data given by Hilsenrath et al. (1960)

$$k_a = 2.411 \times 10^{-2}\,(1 + 3.309 \times 10^{-3}\,T - 1.441 \times 10^{-6}\,T^2).$$

(32)

This gives k_a in watts per meter per degree Celsius for air temperatures between -193 and 277°C.

Figure 5 shows that the noncontinuum effects are, indeed, important, especially to the diffusion of water vapor. In the figure I have plotted D_w' and k_a' as functions of the droplet radius. Even for a radius of 100 μm, D_w' is still 5% below the bulk diffusivity. The effect is less pronounced on the diffusion of heat; k_a' is the same as the bulk thermal conductivity for droplet radii of 5 μm and greater.
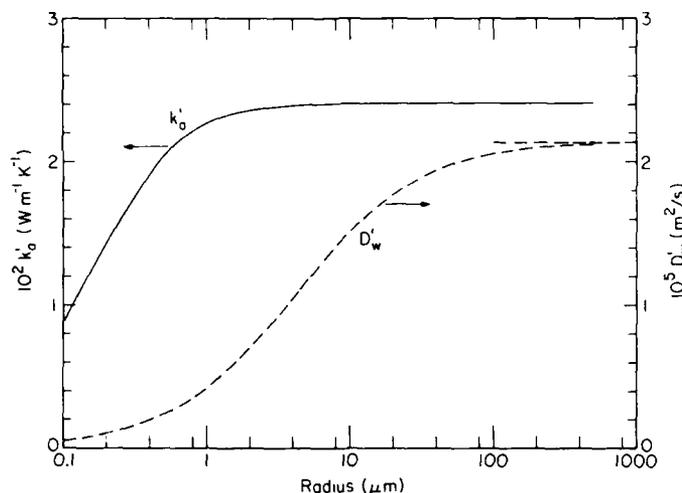
Figure 5. Modified water vapor diffusivity in air (eq 28) and modified thermal conductivity of air (eq 30) as functions of the droplet radius. Conditions are $T = 0\,^\circ C$ *and* $P = 1000\,hPa$.

To find the surface tension of saline water σ_s in eq 7, I use (Pruppacher and Klett 1978, p. 107)

$$\sigma_s = \sigma_w + 2.77 \times 10^{-5}\,(m_s\,/\,m_w) \tag{33}$$

where σ_w is the surface tension of pure water. According to Pruppacher and Klett (1978, p. 104)

$$\sigma_w = 7.610 \times 10^{-2} - 1.55 \times 10^{-4}\,T \tag{34}$$

which gives the surface tension in joules per square meter for a droplet temperature T between –40 and 40°C.

For the latent heat of vaporization of water L_v, which appears in eq 10 and in equations in the next section, I use (Fleagle and Businger 1980, p. 113)

$$L_v = (25.00 - 0.02274\,T) \times 10^5. \tag{35}$$

This gives L_v in joules per kilogram for the droplet temperature T in degrees Celsius.

Finally, to compute the saturation vapor pressure $e_{sat}(T_a)$ at air temperature T_a, I use Buck's (1981) result. For saturation over water at temperature T (in degrees Celsius), he gave

$$e_{sat}\,(T) = (1.0007 + 3.46 \times 10^{-6}\,P)\,6.1121\,\exp\left(\frac{17.502\,T}{240.97 + T}\right). \tag{36}$$

Here the vapor pressure and the atmospheric pressure P are both in hectopascals (which is equivalent to the non-SI unit millibars).

THERMAL EVOLUTION EQUATION

Also in their Chapter 13, Pruppacher and Klett (1978) developed a rate equation for the change in temperature of an aqueous solution droplet. Their result, eq (13-64), is

$$\frac{d}{dt}(T_a - T) = \frac{-3}{r^2 \rho_s c_{ps}}\left[k_a{}'(T_a - T) + L_v D_w{}'(\rho_v - \rho_{vr})\right].$$ (37)

Here c_{ps} is the specific heat of the spray droplet at constant pressure, and ρ_v and ρ_{vr} are the ambient vapor density and the vapor density at the surface of the droplet respectively.

Pruppacher and Klett (1978) assumed that the temperature within a droplet was uniformly T; this is an accurate assumption. We can show this by assuming that there is no fluid motion within a droplet and then using the solution given by Carslaw and Jaeger (1971, p. 233–234) for heat flow in a solid sphere. They found that the time required for a sphere of radius r to be everywhere within 4% of an impulsively applied surface temperature is

$$\tau_h = \frac{0.4\, r^2}{D_h}$$ (38)

where, in our case, $D_h = 1.4 \times 10^{-7}$ m^2/s is the diffusivity of heat in sea water at 0°C (Horne 1969, p. 56). For 1-μm droplets, $\tau_h = 2.9 \times 10^{-6}$ s; for 100-μm droplets, $\tau_h = 2.9 \times 10^{-2}$ s. Later, when I compute the time constants τ_T that characterize the time required for droplets to come to thermal equilibrium in air with temperature T_a, we will see that τ_T is always about 20 times greater than τ_h. Thus, spray droplets are always well mixed with respect to temperature.

The ambient vapor density in eq 37 derives easily from the ideal gas law

$$\rho_v = \frac{100\, M_w\, e_{sat}\,(T_a)}{R\, T_a} f$$ (39)

where f is again the relative humidity. Here the 100 is necessary to yield ρ_v in kilograms per cubic meter when e_{sat} is in hectopascals. I assume that the air at the droplet surface is in vapor equilibrium with the droplet; therefore (Pruppacher and Klett 1978, p. 141)

$$\rho_{vr} = \frac{100\, M_w\, e_{sat}\,(T)}{R\, T} \exp(y)$$ (40)

where $\exp(y)$ gives the relative humidity at the droplet surface.

NUMERICAL METHODS

The purpose of the last two sections was to develop equations with which I could model the size and thermal evolution of sea spray droplets. The resulting equations, eq 10 and 37, both have the form

$$\frac{dx}{dt} = f_x$$ (41)

11

where x is either r or T, and f_x is a function of r, T and environmental parameters such as T_a, f, S and P.

With eq 41, a possible way to model the evolution of x is with a single-step finite difference scheme such as Euler's method. The recursion relation is (Wendroff 1969)

$$x_{n+1} = x_n + \Delta t \, \phi_n \tag{42}$$

where Δt = time step

$\quad x_n$ = current value of x (i.e., at time t_n)

$\quad x_{n+1}$ = predicted value at the next time step

$\quad \phi_n$ = f_{xn}.

On trying this method with eq 10 and 37, however, I found it to diverge before yielding equilibrium values of r and T.

I therefore went to a multi-step Euler method with a predictor–corrector technique (Wendroff 1969) that uses both ϕ_n and ϕ_{n+1} to compute x_{n+1}. The series of recursion relations starts with eq 42. After finding this initial estimate of x_{n+1}, we compute ϕ_{n+1} and then

$$\hat{\phi} = \tfrac{1}{2}(\phi_n + \phi_{n+1}) \, . \tag{43}$$

We next recompute x_{n+1} from

$$x_{n+1} = x_n + \Delta t \, \hat{\phi} \tag{44}$$

and compare this value with the previously computed value to check for convergence. My convergence test is to see whether $|[x_{n+1}(\text{current}) - x_{n+1}(\text{previous})]/x_{n+1}(\text{previous})| \leq 0.0003$. If it is not, I use $x_{n+1}(\text{current})$ to recompute ϕ_{n+1} and repeat the process starting with eq 43.

A complication of my analysis is that I must model the evolution of both r and T simultaneously. Thus, I really have two sets of identical finite-difference equations like eq 41–44 that I must handle together—one for T and one for r. The only essential problem this causes, however, is that the droplet temperature always reaches its equilibrium value (T_{eq}) long before the droplet radius does. At thermal equilibrium, eq 37 shows that

$$T_{eq} = T_a + \frac{L_v D_w{}'}{k_a{}'} (\rho_v - \rho_{vr}) \, . \tag{45}$$

Clearly, since ρ_{vr} is still changing, T changes slowly, though the droplet is in virtual thermal equilibrium with its environment. To model these equilibrium temperature changes, I compute the droplet temperature at time step $n+1$ from

$$T_{n+1} = \frac{1}{2}\left[T_n + T_a + \frac{L_{v,n} D_{w,n}{}'}{k_{a,n}{}'} (\rho_v - \rho_{vr,n}) \right] \tag{46}$$

where the averaging precludes numerical instabilities.

12

The rate at which spray droplets evolve depends on their initial radius. For efficient computing I thus chose the time step Δt according to the initial radius. By trial and error I found that a good initial time step is

$$\Delta t_1 = 10^{\text{Int}\left[\log\left(2 \times 10^5 r_0^2\right)\right]} \tag{47}$$

where r_0 is the initial radius in meters, and Int[] means the integer part of the expression in brackets. This choice does have some physical basis, because the rate at which a droplet exhanges heat and moisture is almost directly proportional to its surface area, $4\pi r^2$. I computed the running time from

$$t_{n+1} = t_n + \Delta t_n. \tag{48}$$

Time steps after the first one are logarithmic; I set them according to

$$\Delta t_n = 0.1\, t_n. \tag{49}$$

To test the equations that Pruppacher and Klett (1978) developed, my evaluations of the physical and chemical variables involved, and the numerical method, I compared the data of El Golli et al. (1974) and Ranz and Marshall (1952) with my model predictions (Fig. 6). El Golli et al. observed the evaporation of saline droplets as they were advected by an air stream through a pipe with controlled temperature and humidity. Although the droplets that El Golli et al. observed had initial radii near the median of sea spray droplets—about 8 μm—their experimental parameters are not especially representative of a sea spray environment. Typically for sea spray, $S = 34$ ‰ and $RH \geq 80\%$. El Golli et al. observed droplets in an environment with $RH = 80\%$, but for these the initial salinity was only 2 ‰ (Fig. 6c). In their highest salinity case, $S = 29$ ‰, the relative humidity was only 29% (Fig. 6a). Fortunately, nothing in the equations that I presented in the *Size Evolution Equation* and *Thermal Evolution Equation* sections makes them exclusively applicable to the high salinity sea spray environment; they should also be accurate at lower salinity.

We must, however, be careful treating low-humidity cases. At low humidity a droplet may lose enough water by evaporation to become saturated with salt. At 0°C, 1 L of pure water can dissolve 0.357 kg of sodium chloride; thus, the maximum molality of a saline solution is 6.11 (see eq 26). Such a saturated solution droplet is in moisture equilibrium with air having a relative humidity of about 75% (Twomey 1954). At lower humidity, the salt will eventually crystallize and the water will all evaporate. For the two low-humidity data sets collected by El Golli et al. (1974) (Fig. 6a and b), I therefore stopped the calculations when enough water had evaporated to increase the droplet molality to 6.11.

One ambiguity that I found in the experimental data of El Golli et al. (1974) is that they reported only one temperature for each set of experimental conditions. They said this was an "average" temperature but did not clarify whether it was the average air temperature in their device, the average droplet temperature during the experimental run, or some other average. In their experiments the droplets were in thermal equilibrium by the time they started observing their evaporation. From eq 45 we see that, because of the evaporation, the droplets could not have been at T_a—they had to be cooler. A second problem with their reporting of the experimental temperature is that the moisture in the air at a given relative humidity is a strong function of the air temperature. Consequently, since El Golli et al. reported RH and some "average" temperature, the comparison depends critically on what I choose for T_a. The conditions given in Figure 6 show the tem-

13
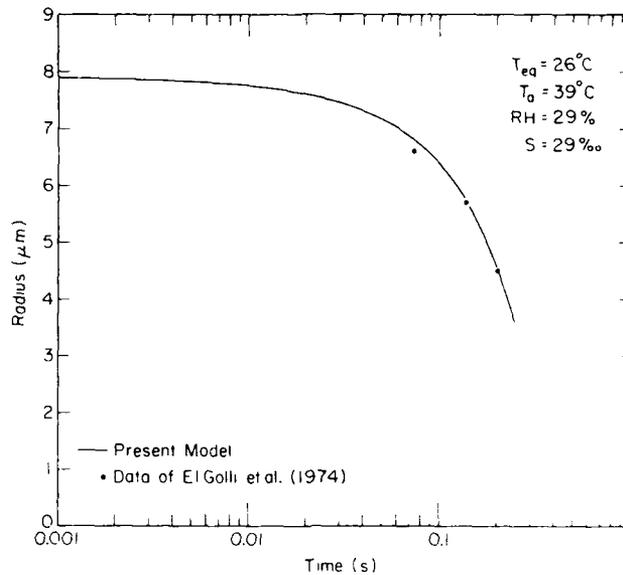
a. Data from Table 2 in El Golli et al. (1974). Model conditions are RH = 29%, S = 29 ‰, T_{eq} = 26 ℃, T_a = 39 ℃ and P = 1000 hPa.
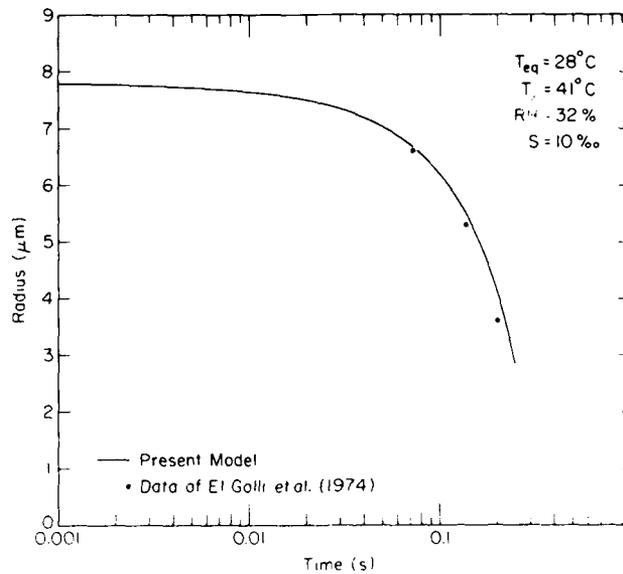
b. Data from Table 3 in El Golli et al. (1974). Model conditions are RH = 32%, S = 10 ‰, T_{eq} = 28 ℃, T_a = 41 ℃, and P = 1000 hPa.

Figure 6. Model computations compared with experimental data.

14
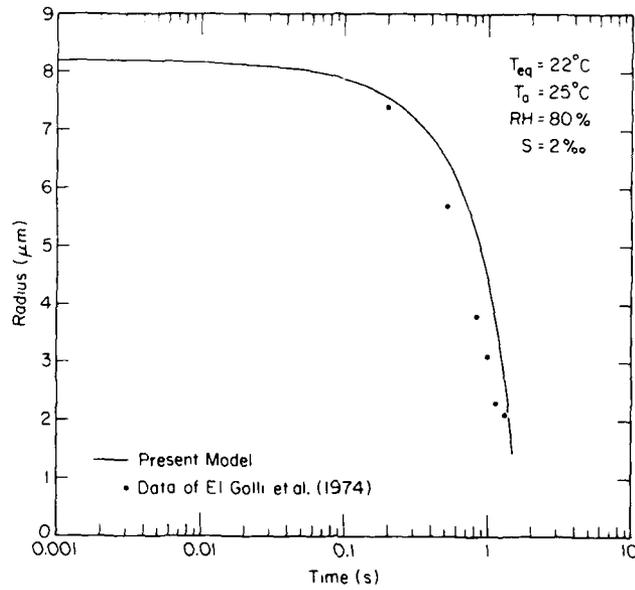
c. *Data from Table 4 in El Golli et al. (1974). Model conditions are* RH = 80%, S = 2 ‰, T_{eq} = 22 °C, T_a = 25 °C *and* P = 1000 hPa.
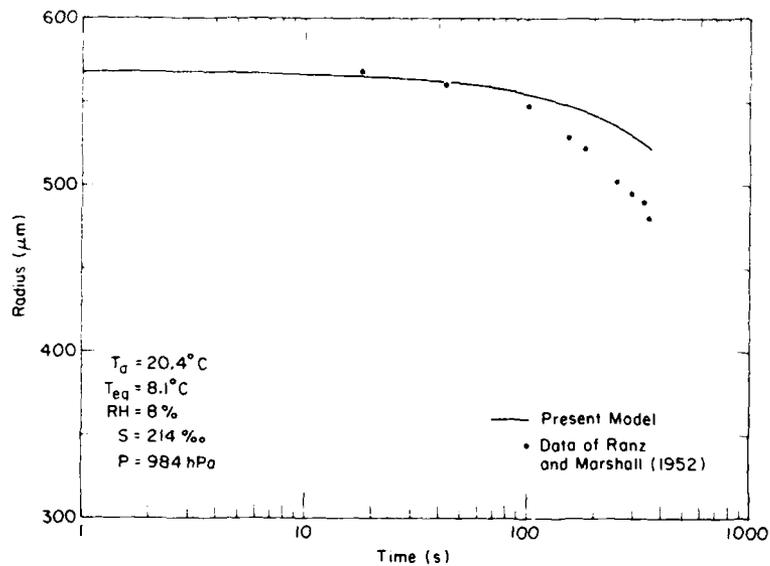
d. *Data from Figure 15b in Ranz and Marshall (1952). Model conditions are* RH = 8%, S = 214 ‰, T_{eq} = 8.1 °C, T_a = 20.4 °C *and* P = 984 hPa.

Figure 6 (cont'd).

15

peratures that yield the best agreement with the data from El Golli et al. It turned out that in my notation their reported "average" temperature is T_{eq}, the droplet temperature at equilibrium. I, thus, chose T_a to yield this T_{eq} value, given the RH and S values reported by El Golli et al.

Aside from Figure 6c, where my model overestimates the experimental droplet size at any given time by about 30%, on average, my model computations agree quite well with the size evolution data reported by El Golli et al. (1974).

Data presented graphically by Ranz and Marshall (1952, their Fig. 15b) provide another important test of my model. Although they considered large and unnaturally saline droplets ($S = 214 \text{‰}$), my model simulates their data well. Figure 6d shows the comparison; my model is always within 9% of their experimental data. Ranz and Marshall did not specify the ambient relative humidity for their experiment but assumed it to be near zero. By trial and error, I found that a relative humidity of 8% produced the best agreement between the model values of T_{eq} and the droplet temperatures measured by Ranz and Marshall.

My analysis of the Ranz and Marshall (1952) data also substantiates some of the underlying physics in my model. Cheng et al. (1988) recently reported producing hollow, spherical salt particles by evaporating sea water droplets in a laboratory and noted that Ranz and Marshall observed similar evaporative particles. Cheng et al. speculated that the hollow spheres might form because sea salts have low diffusivity in water and, thus, might concentrate at the surface of evaporating droplets. My model would be in trouble if this mechanism is at work because it assumes that the salt within the droplet is well mixed. Model simulations of the Ranz–Marshall data, fortunately, repudiate this mechanism and, thus, confirm my assumption that the salt is well mixed. In their Figure 15b, Ranz and Marshall noted that the first salt crystals began forming near a time of 380 s. In my model simulations of their data, the droplet molality reached 6.11—the salt concentration at saturation—near 390 s. (In Figure 6d I plot no data or model results beyond this limit.) This excellent agreement supports my assumption that the salt in the droplets is well mixed. If salt concentrates near the surface of evaporating droplets, as Cheng et al. hypothesized, Ranz and Marshall should have observed crystals forming much earlier.

Using an analysis similar to that given in the *Thermal Evolution Equation* section, I can look closer at the hypothesis by Cheng et al. (1988) that salt diffusion in evaporating droplets is so slow that salt concentrates near the surface. In the *Thermal Evolution Equation* section, I presented Carslaw and Jaeger's (1971, p. 233–234) solution for heat diffusion in a solid sphere. Salt diffusion is an analogous problem. An incremental surface evaporation is equivalent to an incremental injection of salt at the droplet surface. This salt will tend to diffuse throughout the droplet by molecular processes. Unlike the heat diffusion problem in which the surface was clamped at the new temperature, however, the salt will become diluted as it diffuses throughout the droplet; the final concentration will, therefore, be everywhere less than the original surface concentration. Consequently, a time constant like eq 38 will be an upper bound on the time required (τ_s) for a surface salt injection to diffuse throughout the droplet

$$\tau_s < \frac{0.4 \, r^2}{D_s} . \tag{50}$$

Here $D_s = 6.8 \times 10^{-10} \text{ m}^2/\text{s}$ is the molecular diffusivity of NaCl in sea water at 0°C (Horne 1969, p. 56). For 1-μm droplets, $\tau_s < 5.9 \times 10^{-4} \text{ s}$; for 100-$\mu$m droplets, $\tau_s < 5.9 \text{ s}$. We will see

from computations that I will discuss later that these diffusion times are always two orders of magnitude less that the time constant τ_r, which characterizes the time required for sea spray droplets to reach moisture equilibrium with their environment. In other words, salt diffusion within the droplets always seems to be fast enough to maintain a well-mixed interior during sea spray evaporation in a typical marine environment.

With the success of my model in simulating the data from El Golli et al. (1974) and the data and observations of Ranz and Marshall (1952), I feel that we can use it with confidence to investigate the thermal and size evolution of sea spray droplets.

THE GENERATION OF SEA SPRAY

As I hinted in the *Introduction*, sea spray droplets form by three distinct mechanisms. When an air bubble rises to the ocean surface, the bubble cap thins and finally ruptures, throwing micrometer and submicrometer sized *film droplets* into the air. As the bubble cavity then collapses, one to several *jet droplets* shoot into the air from its base. The top jet droplet is about one-tenth the radius of the original bubble; lower jet droplets are generally larger (Blanchard and Syzdek 1988). Blanchard (1963, 1983), Cipriano and Blanchard (1981) and Woolf et al. (1987) discussed these mechanisms; Kientzler et al. (1954), Day (1964) and Resch et al. (1986) showed dramatic photos of bursting bubbles and the resulting spray. When the 10-m wind reaches speeds higher than about 9 m/s, it has the energy to tear off the wave crest and thereby produce *spume droplets* (Monahan et al. 1983). These are typically the largest sea spray droplets, with radii generally greater that 10 μm.

Information on the generation rate of sea spray droplets in a given size range comes from many sources. Monahan (1968), Preobrazhenskii (1973), Monahan et al. (1983) and Wu et al. (1984) reported measurements of the spray droplet size distribution at the sea surface. Wu (1973), Lai and Shemdin (1974), Wang and Street (1978) and Mestayer and Lefauconnier (1988) measured the spray size distribution in wind-wave tunnels. Monahan et al. (1982) measured it in a whitecap simulation tank.

Monahan et al. (1986) synthesized much of these data in a single spray generation function by recognizing that two mechanical processes produce sea spray—bursting bubbles (film and jet droplets) and tearing of wave crests by the wind (spume droplets). Their spray generation function dF/dr_{80} gives the number of spray droplets produced per unit surface area per second per micrometer increment in droplet radius; the units are thus $m^{-2} s^{-1} \mu m^{-1}$ (where number is implicit in the numerator). In dF/dr_{80}, r_{80} denotes that all the observational data were converted to an ambient relative humidity of 80%. Monahan et al. obtained dF/dr_{80} from the sum of two terms

$$\frac{dF}{dr_{80}} = \frac{dF_0}{dr_{80}} + \frac{dF_1}{dr_{80}}$$

(51)

where dF_0/dr_{80} and dF_1/dr_{80} are the contributions from bubble and spume droplets respectively.

For dF_0/dr_{80} Monahan et al. (1986) gave

$$\frac{dF_0}{dr_{80}} = 1.373 U^{3.41} r_{80}^{-3} \left(1 + 0.057 r_{80}^{1.05}\right) 10^{1.19 \exp(-B^2)}$$

(52a)

17

with

$$B = \frac{1}{0.650} (0.380 - \log r_{80}) .$$ (52b)

Here U is the 10-m wind speed in meters per second.

For dF_1/dr_{80}, Monahan et al. (1986) gave

$$\frac{dF_1}{dr_{80}} = 0 \qquad \text{for } r_{80} < 10 \mu m$$ (53a)

$$= 8.60 \times 10^{-6} \exp(2.08 \, U) \, r_{80}^{-2} \quad \text{for } 10 \leq r_{80} < 75 \, \mu m$$ (53b)

$$= 4.83 \times 10^{-2} \exp(2.08 \, U) \, r_{80}^{-4} \quad \text{for } 75 \leq r_{80} < 100 \, \mu m$$ (53c)

$$= 4.83 \times 10^6 \exp(2.08 \, U) \, r_{80}^{-4} \quad \text{for } 100 \, \mu m \leq r_{80} .$$ (53d)

Both eq 52 and 53 are accurate only for a wind speed U that is, nominally, 20 m/s or less.

Because my ultimate interests require that I track the evolution of spray droplets from the instant they form, a spray generation function in terms of r_{80} is inadequate. From dF/dr_{80} I can, however, find dF/dr, the spray generation function in terms of the droplet radius at formation r_0, from

$$\frac{dF}{dr} = \frac{dr_{80}}{dr_0} \frac{dF}{dr_{80}} .$$ (54)

Of course, all the data that Monahan et al. (1986) considered were not obtained at a relative humidity of 80%; to have compatible data sets they had to use a transformation like eq 54 to convert the various observations to a common humidity (they chose 80%). To find dr_{80}/dr_0, Monahan et al. (see also Fairall et al. 1983) used Fitzgerald's (1975) result

$$r_{eq} = \alpha(f) \, r_d^{\beta(f)} .$$ (55)

Here r_{eq} is the equilibrium droplet radius at relative humidity f, r_d is the radius of the dry salt nucleus, and for NaCl

$$\alpha(f) = 1.62 \exp\left(\frac{0.066 f}{g(f) - f}\right)$$ (56)

where

$$g(f) = 1.058 \qquad \text{for } f \leq 097$$ (57a)

$$= 1.058 - \frac{0.0155 \, (f - 0.97)}{1.02 - f^{1.4}} \quad \text{for } 0.97 < f \leq 0.995$$ (57b)

18

and

$$\beta(f) = \exp\left(\frac{0.00077\,f}{1.009 - f}\right) \qquad \text{for } 0.80 \le f \le 0.995 . \tag{58}$$

For eq 58, Fitzgerald gave the lower limit of applicability as $f = 0.81$; but I see nothing in his work to preclude us from extending eq 58 down to $f = 0.80$.

I assume that when spray droplets form, they are injected initially into an environment that is saturated with water vapor—the lowest few centimeters of air near the sea surface. But because the dissolved salts depress the saturation vapor pressure compared to that over a plane surface of pure water, the initial relative humidity is not 100%. Rather, it is (Roll 1965, p. 262; Horne 1969, p. 332)

$$f_0 = 1 - 0.000537\,S \tag{59}$$

where S is the sea surface salinity in parts per thousand.

Knowing this initial humidity, we can use eq 55 to relate r_{80} to r_0 and, thus, find dr_{80}/dr_0. The procedure is to write the two equations

$$r_0 = \alpha(f_0)\,r_d^{\beta(f_0)} \tag{60}$$

$$r_{80} = \alpha(0.8)\,r_d^{\beta(0.8)} \tag{61}$$

and to eliminate r_d. Figure 7 shows r_{80} versus r_0 computed from both Fitzgerald's (1975) equations and from my model. A log-log, least-squares fit of the r_{80}–r_0 data computed with Fitzgerald's equations is

$$r_{80} = 0.5175\,r_0^{0.9756} \tag{62}$$

with both r_{80} and r_0 in micrometers. The least-squares fit to the results from my model is

$$r_{80} = 0.4954\,r_0^{1.0029} . \tag{63}$$

Looking at these two equations and at Figure 7, we see little difference between the two methods of computing r_{80}. But, as Figure 8 shows, there are significant differences between Fitzgerald's (1975) relations and my model. In Figure 8 I plot the ratio r_0/r_{eq} versus r_0 for several values of the ambient relative humidity. Here r_{eq} is the equilibrium radius at the specified humidity; for example, for $RH = 80\%$, $r_{eq} = r_{80}$ and that set of lines in Figure 8 contains the same information as Figure 7. Clearly, in Figure 8, r_0/r_{eq} depends much more on r_0 in Fitzgerald's model than in my model. It is not, however, clear which model is correct. I can only say that I feel mine is because it computes r_{eq} from the fundamental microphysical equations. Fitzgerald's relations, on the other hand, are approximate fits to solutions of the microphysical equations in slightly different form, though he claimed that the approximations are good to within 5%. I also may be extrapolating his results too far; this stated accuracy applies only when r_0 is 10–20 μm or less.

Since my calculations of r_0/r_{eq} yield values that are basically constant over a wide radius range, they have an advantage over computations based on Fitzgerald's (1975) mod-

19
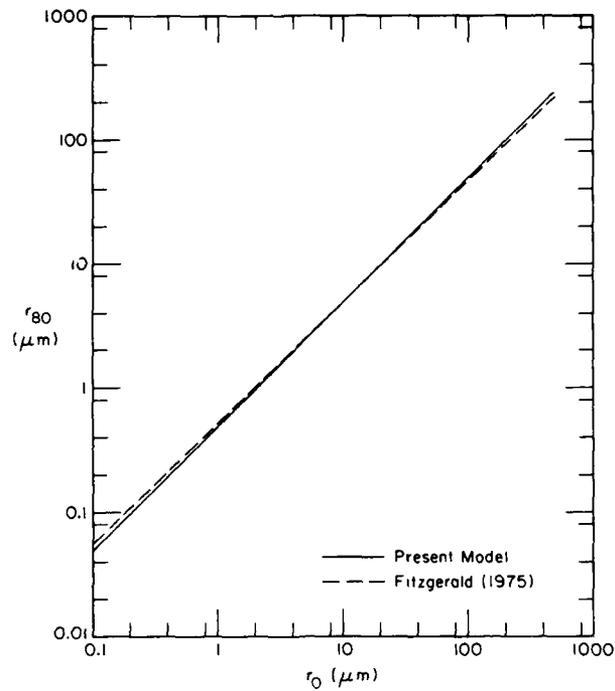
Figure 7. Comparison between r_{80} and r_0 based on Fitzgerald's (1975) relations and on the present model.
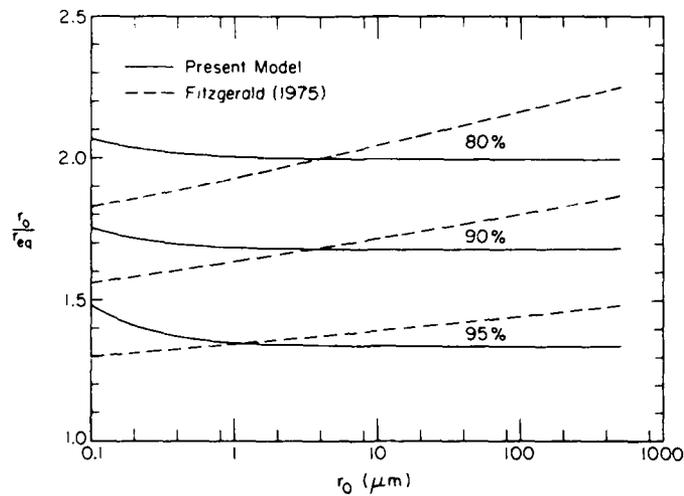
Figure 8. Ratio r_0/r_{eq} computed with Fitzgerald's (1975) relations and with the present model for several values of the ambient relative humidity.

20

el. In fact, Figure 8 provides a rationale for reducing experimental sea spray data to a standard humidity of 80%: at $RH = 80\%$ a spray droplet has a radius that is one-half the droplet radius at formation.

Although computations of r_{80} versus r_0 based on my model seem aesthetically better than those based on Fitzgerald's (1975) model, because Monahan et al. (1986) used Fitzgerald's relations to reduce their experimental data to a common humidity, I defer to the Fitzgerald model in computing dr_{80}/dr_0 for use in eq 54. Therefore, from eq 62

$$\frac{dr_{80}}{dr_0} = 0.5049 r_0^{-0.0244} \ . \tag{64}$$

Using this and eq 51–54, I can compute the rate at which spray droplets are formed as a function of the wind speed. Notice, none of the equations I use for this calculation depend on the humidity, salinity, or air or water temperatures. Some preliminary evidence does, however, suggest that the spray generation function depends on the water temperature.[*] Figure 9 shows dF/dr, the spray generation function, as a function of r_0 and the wind speed. Not unexpectedly, the number of droplets produced with a given radius increases monotonically with the wind speed. This is the bursting bubble mechanism.

Figure 9 also shows clearly that at a wind speed of about 9 m/s a new spray generation mechanism becomes effective. This is spume generation. The wind is now powerful enough to tear off the wave crests and to produce many large spray droplets.

The basic purpose of this section was to identify the size range of spray droplets with which we must be concerned. Figure 9 delineates that size range. Although the spray generation function increases monotonically with decreasing radius in Figure 9, we can call $r_0 = 0.5$ μm a lower limit, because the mass carried by these smallest droplets becomes negligible. Remember, the mass of a spray droplet goes as r_0^3. A reasonable upper size limit is $r_0 = 500$ μm. As I will show later, 500-μm spray droplets remain in the air less than a second before falling back into the sea. Henceforth, I will limit my discussion of sea spray to droplets with an initial radius between 0.5 and 500 μm.

EXAMPLES OF THERMAL AND SIZE EVOLUTION

As I explained in the *Introduction*, I am interested in spray generation associated with polar lows. Since these occur at high northern latitudes, the sea surface temperature T_w is typically 0°C. If the wind is blowing off the pack ice, the air temperature may be as low as –20°C. For southerly winds, the air is warmer; it could reach, say, 5°C. The surface salinity S of the high latitude ocean is commonly about 34 ‰. These are the environmental parameters that I will use for my studies of the thermal and size evolution of sea spray droplets.

Thermal evolution

Figure 10 shows three plots of the evolution of the droplet temperature T with time. I always assume that a spray droplet initially has the temperature of the surface water T_w. T_{eq} is the equilibrium temperature of the droplet in the specified environment and is given by eq 45. In Figure 10 I plot the nondimensional temperature $[T(t)-T_{eq}]/[T_w-T_{eq}]$ as a

---

[*] Personal communication with E. C. Monahan, University of Connecticut, 1987.
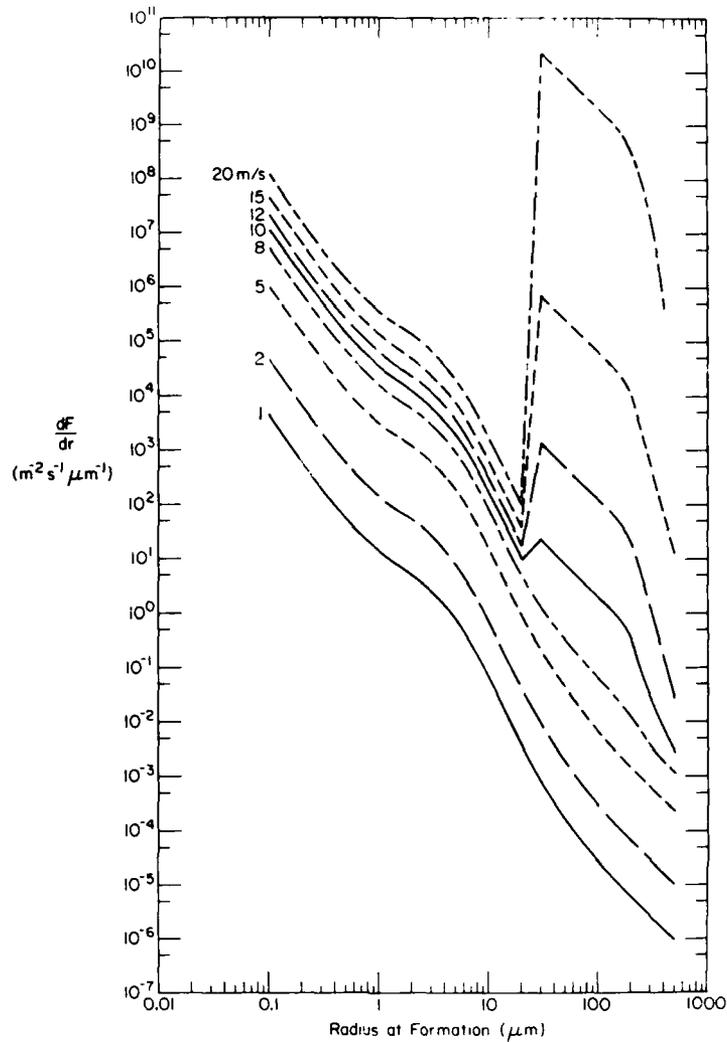
Figure 9. Spray generation function (eq 54) for various values of the 10-m wind speed.

function of the nondimensional time t/τ_T. Here τ_T is a time constant equal to the time required for the spray droplet to reach e^{-1} of its equilibrium temperature. That is

$$\frac{T(\tau_T) - T_{eq}}{T_w - T_{eq}} = e^{-1} .$$

(65)

In the next section I will quantify τ_T.

The thermal evolution depicted in Figure 10 is virtually independent of the relative humidity. The spray droplets reach thermal equilibrium so quickly that no mass has yet been exchanged.

The three droplets modeled in Figure 10 have nearly identical thermal evolution curves. Thus, the basic character of thermal transfer from a sea spray droplet does not de-

22
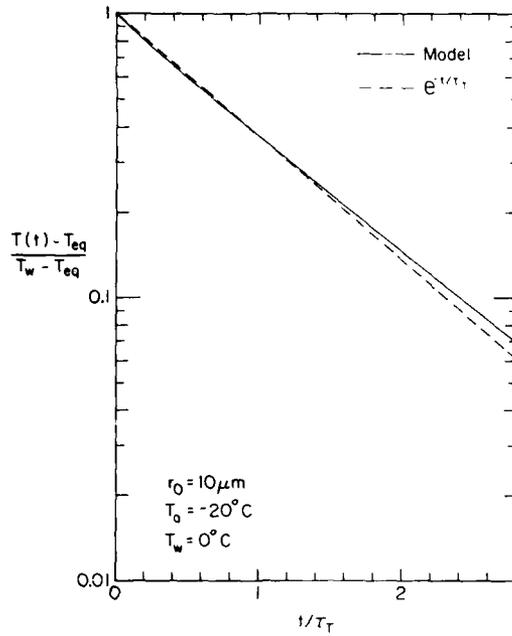
a. $r_0 = 100 \ \mu m, T_a = -10 \, ^\circ C$.
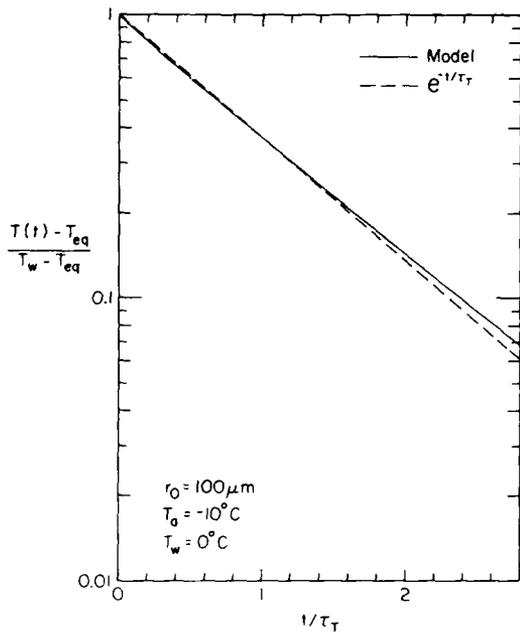
b. $r_0 = 10 \ \mu m, T_a = -20 \, ^\circ C$.
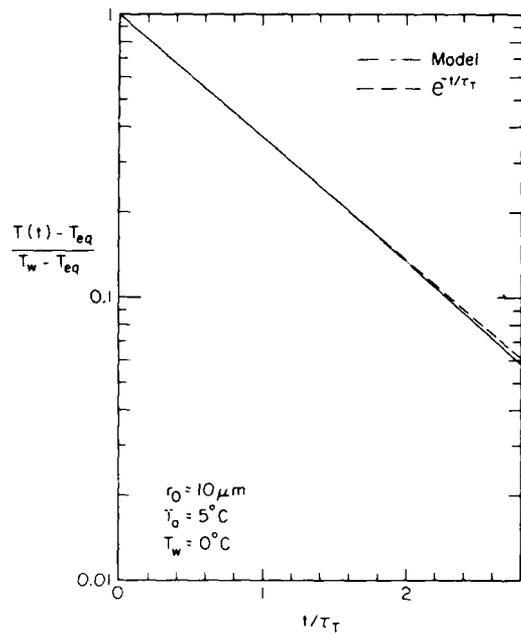
c. $r_0 = 10 \ \mu m, T_a = 5 \, ^\circ C$.

Figure 10. Model calculations of the thermal evolution of spray droplets. Environmental conditions are $T_w = 0 \, ^\circ C$, $S = 34 \ \permil$ *and* $P = 1000 \ hPa$.

23

pend strongly on its size, on its initial temperature or on the ambient temperature and humidity. It does not even depend strongly on the direction of the transfer. In Figure 10c the droplet is warming, and the nondimensional temperature generally falls below the line

$$\frac{T(t) - T_{eq}}{T_w - T_{eq}} = \exp(-t/\tau_T) \ . \tag{66}$$

Although the nondimensional temperature is above this line for the two cooling cases (Fig. 10a and 10b), the deviations from $\exp(-t/\tau_T)$ are not large. Consequently, if we know T_{eq}—which we do from eq 45—and τ_T, $\exp(-t/\tau_T)$ is a fairly accurate model for the thermal evolution of spray droplets, regardless of the environmental conditions (see also Pruppacher and Klett 1978, p. 447).

Size evolution

Figure 11 shows spray droplet size evolution for the three cases shown in Figure 10. In analogy with the temperature, I plot the nondimensional radius $[r(t)-r_{eq}]/[r_0-r_{eq}]$ versus the nondimensional time t/τ_r. Here τ_r is a time constant equal to the time required for the droplet to come to within e^{-1} of its equilibrium radius. That is

$$\frac{r(\tau_r) - r_{eq}}{r_0 - r_{eq}} = e^{-1} \ . \tag{67}$$

I will discuss values of τ_r in the next section.

Figure 11 shows that the size evolution depends strongly on the relative humidity. The lower the relative humidity, the more rapid the moisture exchange at the droplet surface.

Clearly, the model

$$\frac{r(t) - r_{eq}}{r_0 - r_{eq}} = \exp(-t/\tau_r) \tag{68}$$

is not as good for size as it is for droplet temperature. Only for $t/\tau_r \leq 1$ is eq 68 a reasonable model of the droplet radius.

Figure 12 presents the same results shown in Figure 11 but in a form that emphasizes how much a spray droplet actually changes in size and how r_{eq} depends on the relative humidity. The figure, therefore, reiterates some of the information contained in Figure 8: for $RH = 80\%$, $r_0/r_{eq} \approx 2.0$; for $RH = 90\%$, $r_0/r_{eq} \approx 1.7$; and for $RH = 95\%$, $r_0/r_{eq} \approx 1.3$.

On comparing Figures 11 and 12, we see that $r(t)/r_0$ is a more transparent way to non-dimensionalize size evolution than is $[r(t)-r_{eq}]/[r_0-r_{eq}]$; the three plots in Figure 12 are nearly identical despite the diverse conditions that they represent. In Figure 11 the three plots are noticeably different. Evidently, when we parameterize size evolution as $r(t)/r_0$ versus t/τ_r, the initial droplet size and the ambient air and water temperatures do not strongly affect the nature of the moisture transfer. As I will show in the next section, they do, however, affect the rate of the evolution—modeled by τ_r.
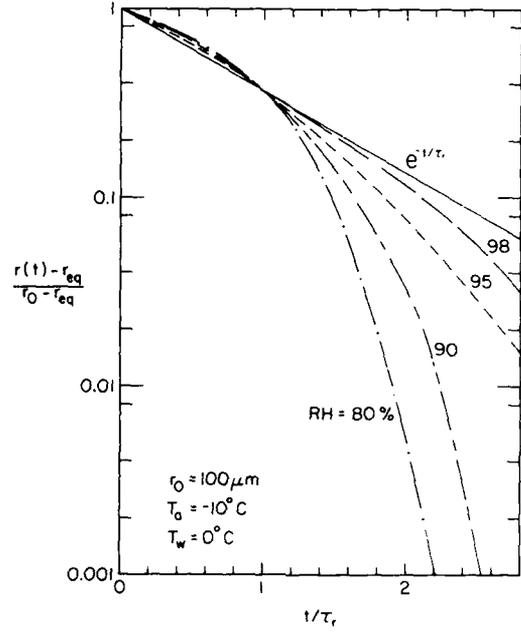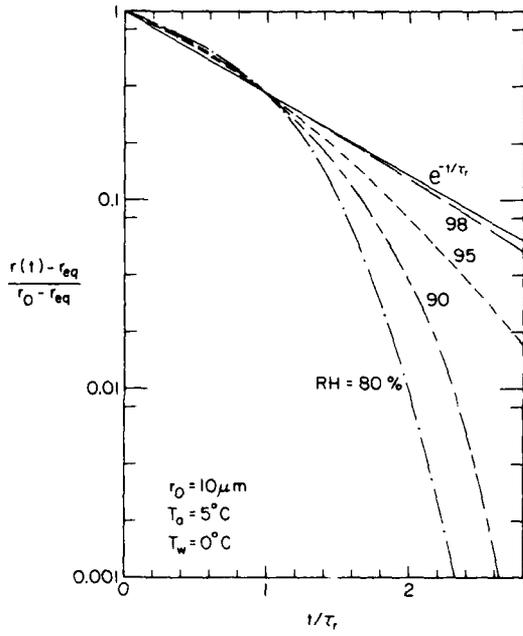
a. $r_0 = 100\ \mu m$, $T_a = -10\,°C$.

b. $r_0 = 10\ \mu m$, $T_a = -20\,°C$.
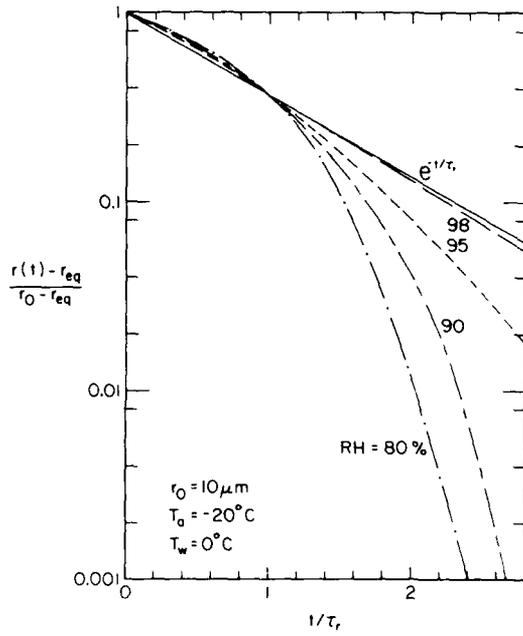
c. $r_0 = 10\ \mu m$, $T_a = 5\,°C$.

Figure 11. Model calculations of the size evolution of spray droplets plotted nondimensionally as $[r(t)-r_{eq}]/[r_0-r_{eq}]$. *Environmental conditions are the same as for Figure 10.*

25
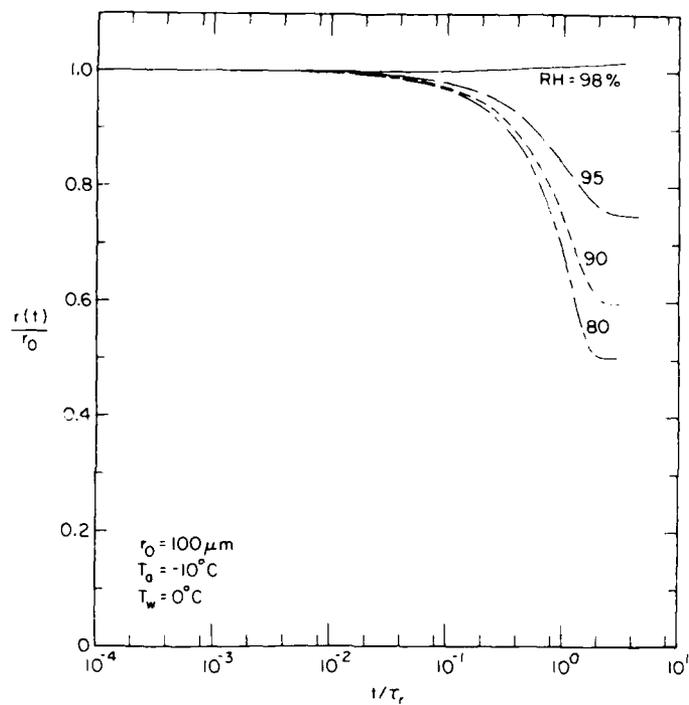
a. $r_0 = 100\ \mu m$, $T_a = -10\,°C$.
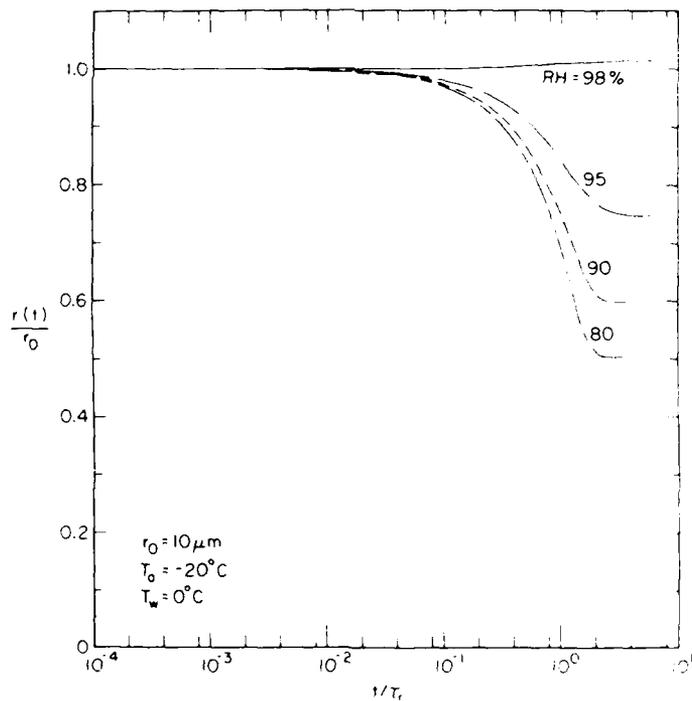
b. $r_0 = 10\ \mu m$, $T_a = -20\,°C$.

Figure 12. Model computations of the size evolution of spray droplets plotted nondimensionally as $r(t)/r_0$. Environmental conditions are the same as for Figure 10.

26
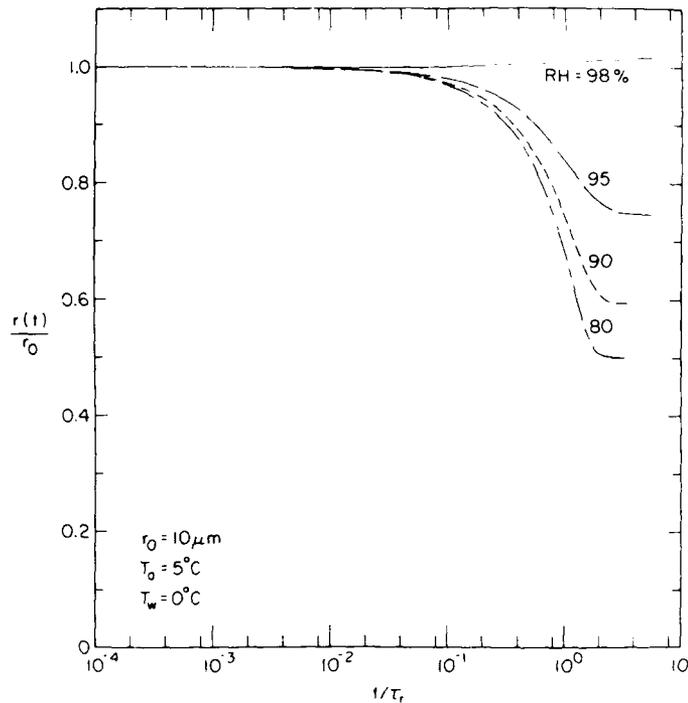
c. $r_0 = 10 \mu m$, $T_a = 5$ °C.

Figure 12 (cont'd).

Figure 12 shows that, when the relative humidity is 98%, the spray droplets grow somewhat, regardless of the direction of the thermal transfer. According to eq 10, droplet growth for $RH = 98\%$ can occur only when

$$y < 0.98 - 1 = -0.02. \tag{69}$$

From eq 7 we can easily demonstrate that y is typically somewhat smaller than –0.02 except for the smallest droplets, for which surface tension is an important effect. Surface tension exerts its influence when the initial droplet radius is about 1 μm or less. Figure 12 will thus not give an accurate picture of the evolution of droplets of this size; when the relative humidity is 98%, they will reach an equilibrium size slightly less than r_0.

TIME CONSTANTS

The time constants τ_T and τ_r that I defined in the last section parameterize how quickly a spray droplet comes to equilibrium with its environment. With my model I can compute τ_T and τ_r for any initial radius and for any set of ambient conditions with $RH > 75\%$. Figure 13 shows plots of τ_T and τ_r for droplets with initial radii from 0.5 to 500 μm and for a host of ambient conditions. Notice the τ_T and τ_r values. A 1-μm droplet is within e^{-1}

27

of its equilibrium temperature in less than 10^{-4} s; a 100-μm droplet, in less than 1 s. A 1-μm droplet is within e^{-1} of its equilibrium radius in about 0.5 s; a 100-μm droplet, in about 1000 s. Clearly, the time constants depend on the droplet radius and on the constituent being exchanged.

The τ_T line in each plot of Figure 13 depends negligibly on the humidity and little on the air or water temperatures. The figure itself explains the lack of humidity dependence. Because τ_T is about three orders of magnitude less than τ_r, moisture exchange at the droplet surface can have no influence on thermal exchange; a droplet reaches thermal equilibrium long before moisture diffusion begins in earnest at the droplet surface. Conversely, because a droplet is in thermal equilibrium with the air long before moisture transfer begins, the initial droplet–air temperature difference can have no effect on that transfer. Hence, the choice of T_w is immaterial to the size evolution calculations.

In each plot in Figure 13, the τ_T line is almost straight on these log–log plots and has a slope of 2. That is,

$$\tau_T \propto r_0^2. \tag{70}$$

a. $T_a = -20\,^\circ C$.   b. $T_a = -10\,^\circ C$.
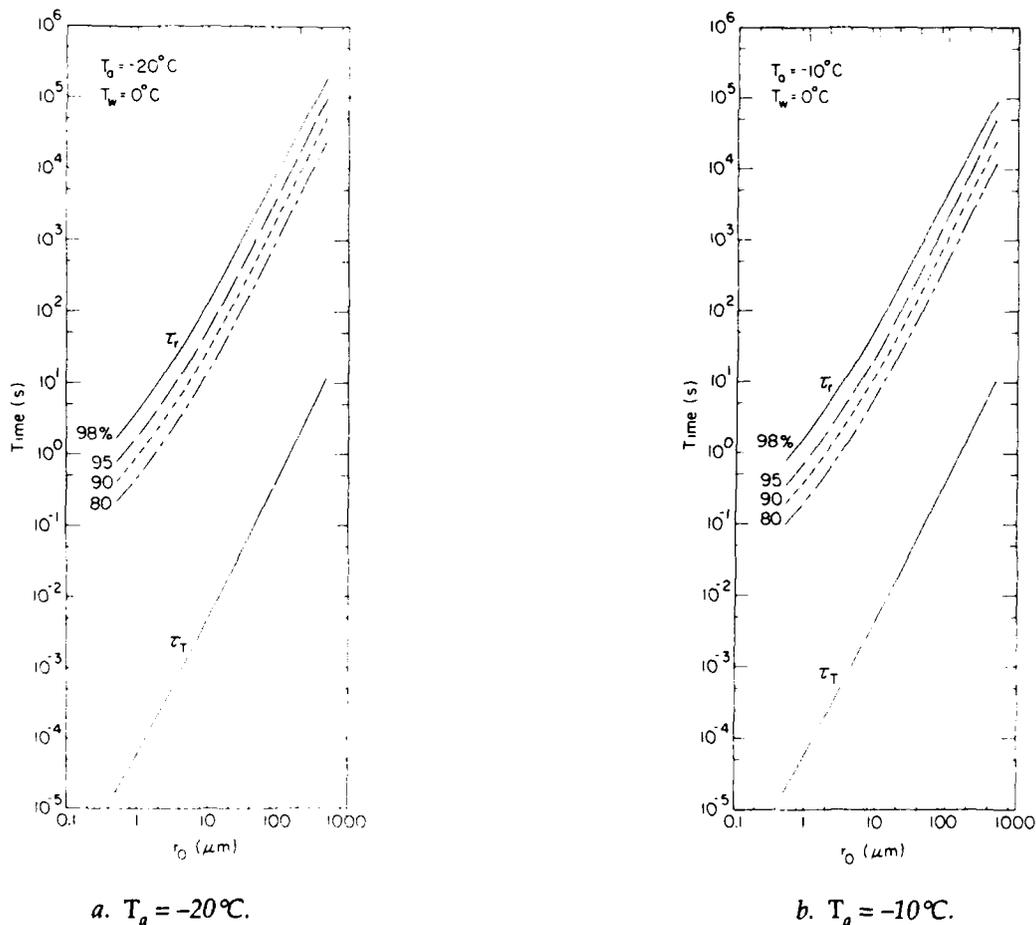
Figure 13. Time constants for thermal (τ_T) and moisture (τ_r) exchange. Environmental conditions are $T_w = 0\,^\circ C$, $S = 34\,\permil$ and $P = 1000$ hPa.

28
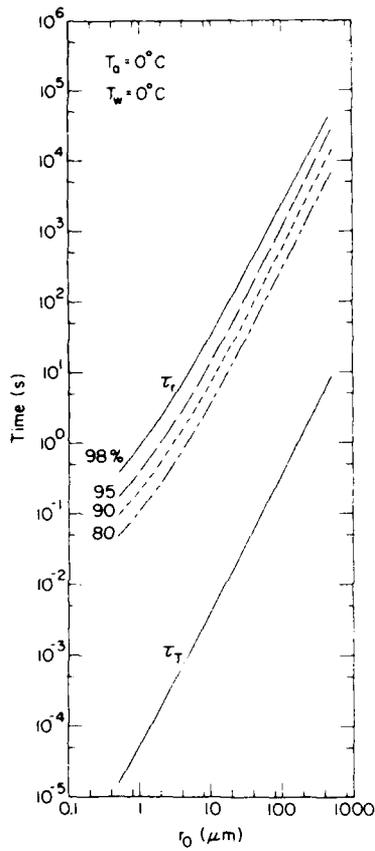
c. $T_a = 0\,°C$.
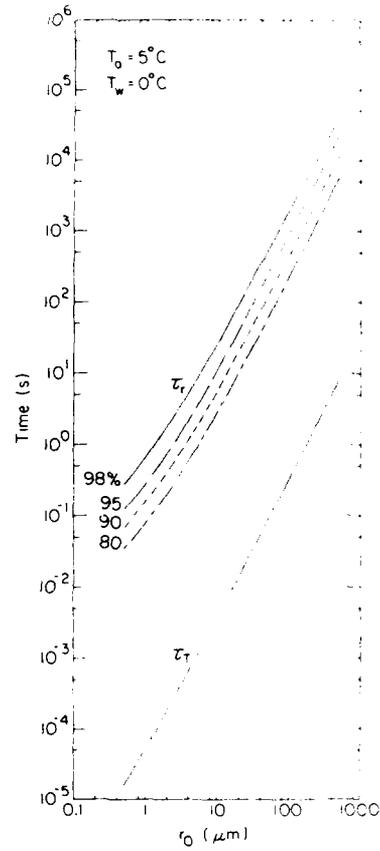
d. $T_a = 5\,°C$.

Figure 13 (cont'd).

Something inherent in the thermal evolution equation must be responsible for this simple result. So consider eq 37 again. From eq 45 we can approximate this as

$$\frac{d}{dt}(T_{eq} - T) = \frac{-3\,k_a{}'}{r_0^2\,\rho_s\,c_{ps}}(T_{eq} - T) \ . \tag{71}$$

The T_{eq} substitution on the right-hand side here is an approximation because L_v and $D_w{}'$ in eq 37 depend on T. Therefore, eq 45 is really valid only when all the variables are evaluated at T_{eq}. In eq 71 I also substituted T_{eq} for T_a on the left-hand side since both are assumed to be independent of time. Because the droplet temperature reaches equilibrium long before any significant moisture transfer occurs, r and $k_a{}'$, which are also time dependent, are essentially constants while a droplet comes to thermal equilibrium. ρ_s, the solution density, is also time dependent in my model; but since that time dependence is through a weak dependence on T, I ignore it, too. Therefore, eq 71 integrates easily to

$$\ln\left[\frac{T(t) - T_{eq}}{T_w - T_{eq}}\right] = \frac{-3\,k_a{}'\,t}{r_0^2\,\rho_s\,c_{ps}} \ . \tag{72}$$

29

When $t = \tau_T$, $[T(\tau_T)-T_{eq}]/[T_w-T_{eq}] = e^{-1}$. Therefore,

$$\frac{-3\,k_a'\,\tau_{Tc}}{r_0^2\,\rho_s c_{ps}} = -1 \tag{73}$$

or

$$\tau_{Tc} = \frac{\rho_s\,c_{ps}\,r_0^2}{3\,k_a'} \ . \tag{74}$$

Here the subscript c denotes that this is a time constant calculated with the approximation eq 74 as opposed to the value τ_T based on the full model.

Figure 14 shows that eq 74 may be an adequate approximation for some applications. In the figure I plot $(\tau_{Tc}-\tau_T)/\tau_T$, which is the relative error in the τ_{Tc} estimate. τ_{Tc} always overestimates τ_T, but the relative error for all radii of interest is less than 50%. For the smallest droplets, that error is even less. Again, these errors result because in reducing eq 37 to eq 74 I made several approximations; most involved ignoring the dependence on the instantaneous droplet temperature of almost all the parameters in eq 37.

In each plot in Figure 13, τ_r increases as the relative humidity increases. The reason is obvious in eq 10. The larger $|f-1|$ is, the faster the rate at which a droplet radius changes.

I have ordered the individual plots in Figure 13 such that 13a has the largest values of τ_r at a given radius and 13d has the smallest. This sequence also reflects air temperatures that go –20, –10, 0, 5°C. The obvious conclusion is that τ_r decreases with an increase in ambient temperature. What's happening physically is that a warmer droplet exchanges vapor with its environment more rapidly than does a cooler one (Bohren 1986). Mathematically, the effect manifests through the $e_{sat}(T_a)$ term in eq 1 and 10.
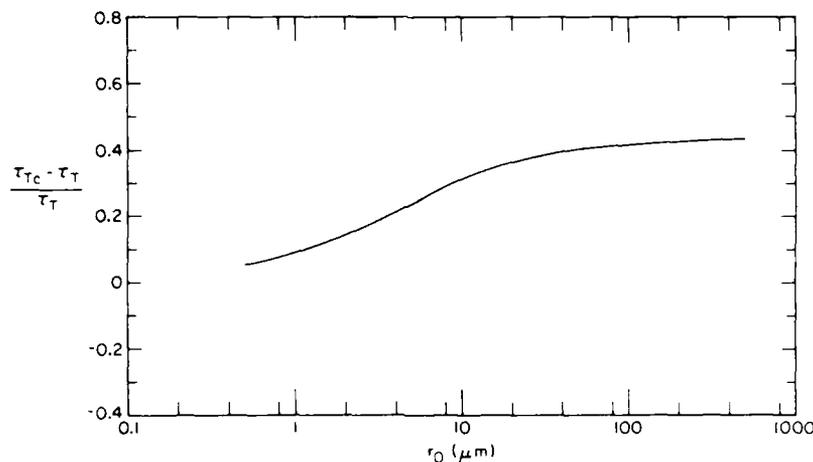
Figure 14. Comparison of calculated (τ_{Tc}, from eq 74) and model (τ_T) values of the time constant for thermal equilibrium. For the model calculations, environmental conditions are $T_w = 0°C$, $T_a = -10°C$, RH = 70% (not important), S = 34 ‰ and P = 1000 hPa. For computing τ_{Tc}, all temperature-dependent parameters were evaluated at 0°C.

30

The largest values for τ_r depicted in Figure 13 are many hours. It is very unlikely that the environment in which sea spray droplets evolve will remain constant this long. And even if the environment remains constant, it is even more unlikely that the largest droplets will stay suspended in the air long enough to approach equilibrium.

We can make a rough estimate of this atmospheric residence time by computing the Stokes fall speed of each droplet. For an atmosphere at rest, the force balance for a spray droplet of radius r is

$$\frac{4}{3} \pi r^3 (\rho_s - \rho_a) g - C_D \rho_a (\pi r^2) u^2 = \frac{4}{3} \pi r^3 \rho_s a \tag{75}$$

where g = acceleration of gravity
  C_D = drag coefficient of the droplet
  u = droplet fall speed
  a = droplet acceleration.

In eq 75 the left-most term is the gravitational force on the droplet—modified by buoyancy effects. The middle term is the frictional drag. The term on the right is the resulting acceleration. When a droplet reaches its terminal fall speed u_f, the right-hand term in eq 75 is zero. Then

$$u_f^2 = \frac{4 r (\rho_s - \rho_a) g}{3 C_D \rho_a} . \tag{76}$$

Schlichting (1968, p. 106) and Batchelor (1970, p. 233) gave the drag coefficient for a sphere as

$$C_D = \frac{6 v_a}{u r} . \tag{77}$$

(Notice, my definition of C_D in eq 76 reflects a value half as large as that used by Schlichting and Batchelor.) The kinematic viscosity of air v_a in eq 77 is a function of the air temperature T_a; to compute v_a for typical sea level pressures near 1000 hPa, I fitted the data of Hilsenrath et al. (1960) with the polynomial

$$v_a(T) = 1.326 \times 10^{-5}(1 + 6.542 \times 10^{-3} T$$

$$+ 8.301 \times 10^{-6} T^2 - 4.840 \times 10^{-9} T^3) . \tag{78}$$

This yields v_a in square meters per second for air temperatures between –173 and 277°C.

Friedlander (1977, p. 105) gave a modified form of the drag coefficient, eq 77, that is more accurate at higher Reynolds numbers

$$C_D = \frac{6 v_a}{u r} (1 + 0.158 Re^{2/3}) . \tag{79}$$

Here the Reynolds number is defined as

$$Re = \frac{2 r u}{v_a} . \tag{80}$$

31

Substituting eq 79 into eq 76 yields an equation in u_f

$$u_f = \frac{2\,r^2\,g}{9\,v_a\left[1 + 0.158(2\,r\,u_f/v_a)^{2/3}\right]}\left(\frac{\rho_s}{\rho_a} - 1\right).$$

(81)

It is routine to solve this equation iteratively for u_f as a function of r_0 by Newton's method.

Figure 15 shows typical values of u_f. Notice, modifying the drag coefficient according to eq 79 is important for the largest droplets; the curvature in the figure at the largest radii indicates that u_f is deviating from the proportionality to r^2 represented at the smaller radii.

In still air, jet droplets generally are projected to no more than 20 cm above the water surface (Blanchard 1963, Bortkovskii 1987). The turbulent air over the ocean will surely lift some of these to greater heights; it will undoubtedly suspend most of the film droplets and may even carry the large spume droplets upward. The spray droplet profiles that de Leeuw (1986, 1987) measured over the open ocean are evidence of this turbulent mixing. His profiles show very little decrease in droplet concentration from the surface to heights of 10–20 m for droplets with radii less than 50 μm, the maximum size he could observe. As it turns out, the fate of spray droplets is one of the unanswered fundamental questions in this field. What is the percentage of droplets that immediately fall back to the surface, and what is the percentage of droplets that remain suspended by the turbu-
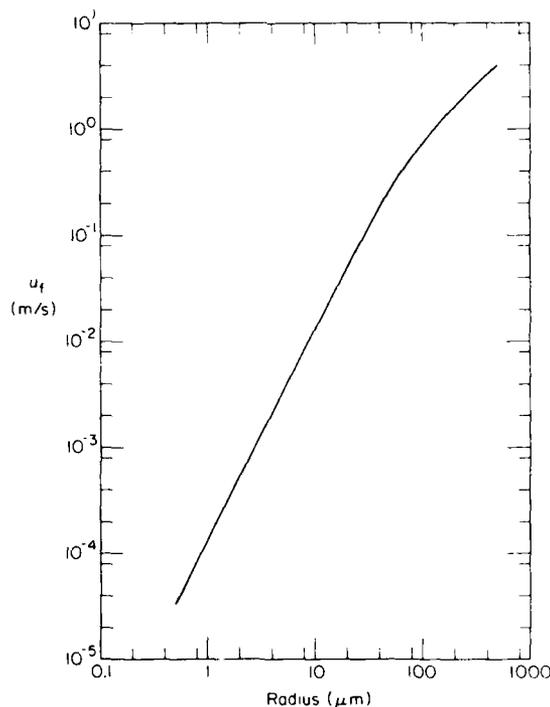
Figure 15. Values of the terminal fall speed computed from eq 81. Environmental conditions are $T_a = -10\,°C$, $S = 34\,‰$ and $P = 1000\,hPa$.

lence and, thus, approach their full thermodynamic potential? Turbulence modeling of the marine surface layer like that begun by Fairall et al. (1987) is vital to addressing these questions.

It is therefore an oversimplification to base spray droplet residence times only on the terminal fall speed. If the fall speed is less than typical turbulent vertical velocity fluctuations—nominally 0.2–0.3 m/s in a 10-m/s wind—the turbulence may suspend the particles indefinitely. According to Figure 15, droplets with radii less than about 50 μm have terminal fall speeds less than this limit. Only for the largest droplets—for which the fall speed is much greater than the turbulent velocity fluctuations—can we be certain that the physics contained in eq 75 is sufficient.

The terminal fall speed, nevertheless, does give us an intuitive feel for the atmospheric residence times. In Figure 16 I thus plot a time constant or residence time τ_f, which is the time required for a droplet of radius r_0 to fall 1 m in still air. That is,

$$\tau_f = \frac{1}{u_f} . \tag{82}$$

For comparison, in the figure I also plot the τ_T values and two sets of the τ_r values from Figure 13b. We see that many of the spray droplets—namely, those with radii greater than about 20 μm—will probably fall back into the sea before reaching their equilibrium radius. Because of the rapidity of the thermal exchange, however, all but the very largest spray droplets should reach thermal equilibrium before falling back to the surface.
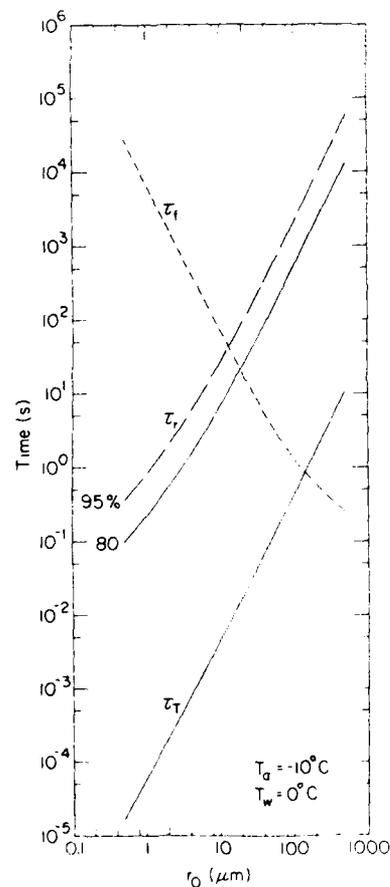
Figure 16. Time constants for thermal (τ_T) and moisture (τ_r) exchange and the time required for a droplet to fall 1 m in still air (τ_f). Environmental conditions are $T_w = 0\,°C$, $T_a = -10\,°C$, $S = 34\,‰$ and $P = 1000$ hPa.

33

CONCLUSIONS

The equations that I have presented constitute a powerful model for treating many problems related to the evolution of sea spray droplets. I have shown a few applications here, such as modeling how droplets approach thermal and moisture equilibrium and finding time constants characterizing these processes. An important conclusion of these modeling runs is the disparity between the time constants for thermal (τ_T) and moisture (τ_r) equilibrium. Although both τ_T and τ_r increase with the initial spray droplet radius roughly as r_0^2, at a given radius τ_r is always at least three orders of magnitude larger than τ_T for humidities typical over the high latitude ocean. Consequently, the ambient relative humidity has negligible effect on the thermal evolution of spray droplets; and the air–sea temperature difference has minimal impact on their moisture evolution.

Although all the computations I discussed were for a steady-state environment, the model can easily handle droplet evolution in a changing environment. This capability will allow us, in the future, to treat not just single, isolated spray droplets but also a cloud of interacting droplets. The groundwork is now in place for our research on the role of sea spray in the air–sea exchange of heat and moisture.

LITERATURE CITED

Andreas, E.L, R.M. Williams and C.A. Paulson (1981) Observations of condensate profiles over Arctic leads with a hot-film anemometer. *Quarterly Journal of the Royal Meteorological Society*, **107**: 437–460.

Batchelor, G.K. (1970) *An Introduction to Fluid Dynamics.* Cambridge: Cambridge University Press.

Blanchard, D.C. (1963) The electrification of the atmosphere by particles from bubbles in the sea. In *Progress in Oceanography* (M. Sears, Ed.). New York: MacMillan, p. 71–202.

Blanchard, D.C. (1983) The production, distribution, and bacterial enrichment of the sea-salt aerosol. In *Air–Sea Exchange of Gases and Particles* (P.S. Liss and W.G.N. Slinn, Eds.). Dordrecht: D. Reidel, p. 407–454.

Blanchard, D.C. and L.D. Syzdek (1988) Film drop production as a function of bubble size. *Journal of Geophysical Research*, **93**: 3649–3654.

Bohren, C.F. (1986) Sugar and spice: The dirty wet-bulb temperature. *Weatherwise*, **39**: 46–50.

Borisenkov, E.P. (1974) Some mechanisms of atmosphere–ocean interaction under stormy weather conditions. *Problems of the Arctic and the Antarctic*, **43-44**: 73–83.

Bortkovskii, R.S. (1973) On the mechanism of interaction between the ocean and the atmosphere during a storm. *Fluid Mechanics—Soviet Research*, **2**: 87–94.

Bortkovskii, R.S. (1987) *Air-Sea Exchange of Heat and Moisture During Storms.* Dordrecht: D. Reidel.

Buck, A.L. (1981) New equations for computing vapor pressure and enhancement factor. *Journal of Applied Meteorology*, **20**: 1527–1532.

Carslaw, H.S. and J.C. Jaeger (1971) *Conduction of Heat in Solids*, 2nd Edition. London: Oxford University Press.

Cheng, R.J., D.C. Blanchard and R.J. Cipriano (1988) The formation of hollow sea-salt particles from the evaporation of drops of seawater. *Atmospheric Research*, **22**: 15–25.

Cipriano, R.J. and D.C. Blanchard (1981) Bubble and aerosol spectra produced by a laboratory "breaking wave." *Journal of Geophysical Research*, **86**: 8085–8092.

Cipriano, R.J., E.C. Monahan, P.A. Bowyer and D.K. Woolf (1987) Marine condensation nucleus generation inferred from whitecap simulation tank results. *Journal of Geophysical Research*, 92: 6569–6576.

Day, J.A. (1964) Production of droplets and salt nuclei by bursting air-bubble films. *Quarterly Journal of the Royal Meteorological Society*, 90: 72–78.

De Leeuw, G. (1986) Vertical profiles of giant particles close above the sea surface. *Tellus*, 38B: 51–61.

De Leeuw, G. (1987) Near-surface particle size distribution profiles over the North Sea. *Journal of Geophysical Research*, 92: 14,631–14,635.

El Golli, S., J. Bricard, P.-Y. Turpin and C. Treiner (1974) The evaporation of saline droplets. *Aerosol Science*, 5: 273–292.

Fairall, C.W., K.L. Davidson and G.E. Schacher (1983) An analysis of the surface production of sea-salt aerosols. *Tellus*, 35B: 31–39.

Fairall, C.W., J.B. Edson and M.A. Miller (1987) Heat fluxes, whitecaps, and sea spray. Technical Report. Department of Meteorology, Pennsylvania State University, University Park, Pennsylvania.

Fitzgerald, J.W. (1975) Approximation formulas for the equilibrium size of an aerosol particle as a function of its dry size and composition and the ambient relative humidity. *Journal of Applied Meteorology*, 14: 1044–1049.

Fleagle, R.G. and J.A. Businger (1980) *An Introduction to Atmospheric Physics*, 2nd Edition. New York: Academic Press.

Friedlander, S.K. (1977) *Smoke, Dust and Haze: Fundamentals of Aerosol Behavior*. New York: John Wiley and Sons.

Hilsenrath, J., C.W. Beckett, W.S. Benedict, L. Fano, H.J. Hoge, J.F. Masi, R.L. Nuttall, Y.S. Touloukian and H.W. Woolley (1960) *Tables of Thermodynamic Transport Properties of Air, Argon, Carbon Dioxide, Carbon Monoxide, Hydrogen, Nitrogen, Oxygen, and Steam*. Oxford: Pergamon Press.

Horne, R.A. (1969) *Marine Chemistry*. New York: Wiley-Interscience.

Kellogg, W.W. and P.F. Twitchell (1986) Summary of the Workshop on Arctic Lows, 9–10 May 1985, Boulder, Colorado. *Bulletin of the American Meteorological Society*, 67: 186–193.

Kientzler, C.F., A.B. Arons, D.C. Blanchard and A.H. Woodcock (1954) Photographic investigation of the projection of droplets by bubbles bursting at a water surface. *Tellus*, 6: 1–7.

Lai, R.J. and O.H. Shemdin (1974) Laboratory study of the generation of spray over water. *Journal of Geophysical Research*, 79: 3055–3063.

Ling, S.C. and T.W. Kao (1976) Parameterization of the moisture and heat transfer process over the ocean under whitecap sea states. *Journal of Physical Oceanography*, 6, 306–315.

Ling, S.C., A. Saad and T.W. Kao (1978) Mechanics of multiphase fluxes over the ocean. In *Turbulent Fluxes through the Sea Surface, Wave Dynamics, and Prediction* (A. Favre and K. Hasselmann, Eds.). New York: Plenum Press, p. 185–194.

Low, R.D.H. (1969a) A generalized equation for the solution effect in droplet growth. *Journal of the Atmospheric Sciences*, 26: 608–611.

Low, R.D.H. (1969b) A theoretical study of nineteen condensation nuclei. *Journal de Recherches Atmospheriques*, 4: 65–78.

Mason, B.J. (1957) The oceans as a source of cloud-forming nuclei. *Geofisica Pura e Applicata*, 36: 148–155.

Mestayer, P. and C. Lefauconnier (1988) Spray droplet generation, transport, and evapo-ration in a wind wave tunnel during the Humidity Exchange over the Sea Experiments in the Simulation Tunnel. *Journal of Geophysical Research*, **93**: 572–586.

Millero, F.J. (1972) The partial molal volumes of electrolytes in aqueous solutions. In *Water and Aqueous Solutions* (R.A. Horne, Ed.). New York: Wiley-Interscience, p. 519–595.

Monahan, E.C. (1968) Sea spray as a function of low elevation wind speed. *Journal of Geophysical Research*, **73**: 1127–1137.

Monahan, E.C. (1971) Oceanic whitecaps. *Journal of Physical Oceanography*, **1**: 139–144.

Monahan, E.C. and I. O Muircheartaigh (1981) Improved statement of the relationship between surface wind speed and oceanic whitecap coverage as required for the interpre-tation of satellite data. In *Oceanography from Space* (J.F.R. Gower, Ed.). New York: Plenum Press, p. 751–755.

Monahan, E.C., K.L. Davidson and D.E. Spiel (1982) Whitecap aerosol productivity de-duced from simulation tank measurements. *Journal of Geophysical Research*, **87**: 8898–8904.

Monahan, E.C., C.W. Fairall, K.L. Davidson and P.J. Boyle (1983) Observed inter-relations between 10 m winds, ocean whitecaps and marine aerosols. *Quarterly Journal of the Royal Meteorological Society*, **109**: 379–392.

Monahan, E.C., D.E. Spiel and K.L. Davidson (1986) A model of marine aerosol genera-tion via whitecaps and wave disruption. In *Oceanic Whitecaps and Their Role in Air–Sea Ex-change Processes* (E.C. Monahan and G. Mac Niocaill, Eds.). Dordrecht: D. Reidel, p. 167–174.

Neumann, G. and W.J. Pierson, Jr. (1966) *Principles of Physical Oceanography*. Englewood Cliffs, New Jersey: Prentice-Hall.

Preobrazhenskii, L.Yu (1973) Estimate of the content of spray-drops in the near-water layer of the atmosphere. *Fluid Mechanics—Soviet Research*, **2**: 95–100.

Pruppacher, H.R. and J.D. Klett (1978) *Microphysics of Clouds and Precipitation*. Dordrecht: D. Reidel.

Ranz, W.E. and W.R. Marshall, Jr. (1952) Evaporation of drops, Part II. *Chemical Engineer-ing Progress*, **48**: 173–180.

Rasmussen, E. (1985) A case study of a polar low development over the Barents Sea. *Tel-lus*, **37A**: 407–418.

Rasmussen, E. and M. Lystad (1987) The Norwegian Polar Lows Project: A summary of the International Conference on Polar Lows, 20–23 May 1986, Oslo, Norway. *Bulletin of the American Meteorological Society*, **68**: 801–816.

Resch, F.J., J.S. Darrozes and G.M. Afeti (1986) Marine liquid aerosol production from bursting of air bubbles. *Journal of Geophysical Research*, **91**: 1019–1029.

Roll, H.U. (1965) *Physics of the Marine Atmosphere*. New York: Academic Press.

Schacher, G.E., K.L. Davidson, C.W. Fairall and D.E. Spiel (1981) Calculation of optical extinction from aerosol spectral data. *Applied Optics*, **20**: 3951–3957.

Schlichting, H. (1968) *Boundary-Layer Theory*, 6th Edition. New York: McGraw-Hill.

Shapiro, M.A., L.S. Fedor and T. Hampel (1987) Research aircraft measurements of a po-lar low over the Norwegian Sea. *Tellus*, **39A**: 272–306.

Street, R.L., C.S. Wang, D.A. McIntosh and A.W. Miller, Jr. (1978) Fluxes through the boundary layers at an air–water interface: laboratory studies. In *Turbulent Fluxes through the Sea Surface, Wave Dynamics, and Prediction* (A. Favre and K. Hasselmann, Eds.). New York: Plenum Press, p. 99–118.

Twomey, S. (1954) The composition of hygroscopic particles in the atmosphere. *Journal of Meteorology*, **11**: 334-338.

Wang, C.S. and R.L. Street (1978) Transfer across an air–water interface at high wind speeds: the effect of spray. *Journal of Geophysical Research*, **83**: 2959–2969.

Wendroff, B. (1969) *First Principles of Numerical Analysis*. Reading, Massachusetts: Addison-Wesley.

Woodcock, A.H. (1952) Atmospheric salt particles and raindrops. *Journal of Meteorology*, **9**: 200–212.

Woodcock, A.H. (1978) Marine fog droplets and salt nuclei—Part I. *Journal of the Atmospheric Sciences*, **34**: 657–664.

Woolf, D.K., P.A. Bowyer and E.C. Monahan (1987) Discriminating between film drops and jet drops produced by a simulated whitecap. *Journal of Geophysical Research*, **92**: 5142–5150.

Wu, J. (1973) Spray in the atmospheric surface layer: laboratory study. *Journal of Geophysical Research*, **78**: 511–519.

Wu, J. (1974) Evaporation due to spray. *Journal of Geophysical Research*, **79**: 4107–4109.

Wu, J. (1979) Spray in the atmospheric surface layer: review and analysis of laboratory and oceanic results. *Journal of Geophysical Research*, **84**: 1693–1704.

Wu, J., J.J. Murray and R.J. Lai (1984) Production and distributions of sea spray. *Journal of Geophysical Research*, **89**: 8163–8169.

A facsimile catalog card in Library of Congress MARC format is reproduced below.

Andreas, Edgar L
    Thermal and size evolution of sea spray droplets / by Edgar L Andreas. Hano-
ver, N.H.: U.S. Army Cold Regions Research and Engineering Laboratory;
Springfield, Va.: available from National Technical Information Service, 1989.
    vii, 48 p., illus., 28 cm. (CRREL Report 89-11.)
    Bibliography: p. 34.
    1. Air–sea interaction. 2. Bubbles. 3. Heat transfer. 4. Microphysics. 5. Moisture
transfer. 6. Polar lows. 7. Sea spray. 8. Water droplets. 9. Whitecaps. I. Andreas,
Edgar L. II. United States Army. III. Corps of Engineers. IV. Cold Regions Re-
search and Engineering Laboratory. V. Series: CRREL Report 89-11.